

Research paper

New telmisartan-derived PPAR γ agonists: Impact of the 3D-binding mode on the pharmacological profileVictoria Obermoser^a, Margarethe E. Urban^b, Manuela S. Murgueitio^c, Gerhard Wolber^c, Ulrich Kintscher^d, Ronald Gust^{a,*}^a Pharmaceutical Chemistry, Institute of Pharmacy, Universität Innsbruck, Innrain 80-82, 6020, Innsbruck, Austria^b Pharmaceutical Chemistry, Institute of Pharmacy, Freie Universität Berlin, Königin-Luise Str. 2+4, 14195, Berlin, Germany^c Computer-Aided Drug Design, Institute of Pharmacy, Freie Universität Berlin, Königin-Luise Str. 2+4, 14195, Berlin, Germany^d Institute of Pharmacology, Center for Cardiovascular Research, Charité Universitätsmedizin Berlin, Hessische Str. 3-4, 10115, Berlin, Germany

ARTICLE INFO

Article history:

Received 23 June 2016

Received in revised form

12 August 2016

Accepted 13 August 2016

Available online 15 August 2016

Keywords:

PPAR γ

Transactivation

Cytotoxicity

Binding mode

Molecular modeling

ABSTRACT

In previous studies, the 4'-((2-propyl-1H-benzo[d]imidazol-1-yl)methyl)-[1,1'-biphenyl]-2-carboxylic acid was identified as pharmacophoric core for PPAR γ activation. In this structure-activity relationship study the C2-alkyl chain was elongated and the 2-COOH group was changed to a carbamide/carbonitrile or shifted to the 3- or 4-position. Furthermore, the benzo[d]imidazole was exchanged by 2,3-dihydrobenzo[d]thiazole or 1H-indole. C2-propyl derivatives showed the profile of partial agonists, while elongation of the C2-chain to that of an n-heptyl group or a 4-COOH shift changed the pharmacological profile to that of a potent full agonist. This finding can be explained by binding to the LBD in different ligand conformations. Two anchoring points (Tyr473 and Arg288) exist in the LBD, which have to be contacted to achieve receptor activation. In a crystal violet chemosensitivity assay using COS-7 cells and LNCaP cells expressing PPAR γ only the carbamide derivatives influenced the cell growth, independently on the presence of the PPAR γ . Therefore, receptor mediated cytotoxicity can be excluded.

© 2016 Elsevier Masson SAS. All rights reserved.

1. Introduction

The peroxisome proliferator-activated receptor γ (PPAR γ) belongs to the hormone receptor superfamily of ligand-activated transcription factors whose activity is regulated by direct binding of hormones (steroids and iodothyronines), lipid metabolites, vitamins and various xenobiotics [1].

Activation of PPAR γ leads to a conformational change, followed by a heterodimerization with retinoic X receptors (RXRs), dissociation of corepressors and recruitment of coactivators [2]. Subsequently, the heterodimer binds to sequence-specific DNA response

elements (PPRE) in enhancer sites of target genes and regulates gene transcription [3].

PPAR γ is one of the main regulators of adipogenesis, glucose and lipid homeostasis and its activation has beneficial effects on serum glucose levels [4].

Synthetic high-affinity ligands for PPAR γ are e.g. the thiazolidinediones (TZDs), which act as so-called insulin-sensitizers and were broadly used in the therapy of type II diabetes mellitus and the metabolic syndrome. However, severe side effects like weight gain, body fluid retention, congestive heart failure and loss of bone mineral density go along with full activation of PPAR γ [5], which led to withdrawal from the market or limited usage of all initially approved TZDs [6–8].

Aside from these well-known and well-investigated metabolic actions triggered by PPAR γ activation, target genes of PPAR γ are also involved in cellular differentiation, development of various organs, and carcinogenesis [9]. It was suggested that activation of PPAR γ induces apoptosis in several malignant cell lines [10] and promotes terminal differentiation of tumor cells [11]. *In vitro* studies already demonstrated antiproliferative and proapoptotic actions in prostate cancer for PPAR γ agonists out of the TZD class

Abbreviations: A_{max}, maximum intrinsic activity; BPO, benzoyl peroxide; DMEM, Dulbecco's modified Eagle medium; LBD, ligand binding domain; mp, melting point; NBS, N-bromosuccinimide; PPAR, peroxisome proliferator-activated receptor; PPRE, peroxisome proliferator-activated receptor response element; RT, room temperature; SAR, structure-activity relationship; SD, standard deviation; TG, triglyceride; TZD, thiazolidinedione.

* Corresponding author.

E-mail address: ronald.gust@uibk.ac.at (R. Gust).

[12]. Additionally, inhibition of tumorigenesis upon activation of PPAR γ was also shown *in vivo* in many animal cancer models [13].

These findings are of high interest, because human prostate cancer tissue expresses PPAR γ at high levels, while healthy human prostate tissue expresses PPAR γ only at low levels [14,15]. This different expression of PPAR γ can probably be used to develop agonists suitable for the tumor-specific treatment of the prostate cancer. For this purpose, however, the side effects not related to tumor therapy have to be minimized.

In recent years, the concept of disconnecting the potency of agonism of PPAR γ and efficacy has been developed in terms of selective modulation or partial activation of the PPAR γ as some side effects might be related to the classic agonistic activity of TZDs.

Full agonists replace helix H12 in a conformation promoting the interaction with coactivators [16], while partial agonists activate the PPAR γ via a mechanism that is independent from helix H12 [17]. In addition, it is conceivable not to seek for compounds with higher potency and efficacy but to look for compounds with a differential mechanism of action, e.g. alterations in the phosphorylation pattern of PPAR γ [18].

Telmisartan, an angiotensin type 1 (AT1) receptor antagonist commonly used in antihypertensive therapy, was reported to act as a partial agonist of PPAR γ *in vitro*. It demonstrated to have a specific coregulator recruitment profile compared to the TZDs, which translated to a different gene expression pattern [19–21]. In animal studies, telmisartan proved to have a positive impact on plasma glucose levels and insulin sensitivity by simultaneously preventing from TZD-alike side effects [20,21]. In further studies, telmisartan was found to have growth inhibitory effects on various cancer cell lines of the urogenital tract via a PPAR γ -mediated pathway [22,23].

This interesting pharmacological profile induced us to select telmisartan as lead structure. In structure-activity relationship (SAR) studies we elucidated the 4'-((2-propyl-1*H*-benzo[d]imidazol-1-yl)methyl)-[1,1'-biphenyl]-2-carboxylic acid (**1-A**) as essential scaffold to meet the minimum requirements for PPAR γ activation with the same potency as telmisartan [24].

Substituents at position 5 were already introduced at the benzo[d]imidazole and shifted to position 6, showing that both, type and position of the substituent, have a strong influence on the compound's PPAR γ activity [25,26].

The C2-substituent influences potency and efficacy [27]. In this study, we elucidate if the successive elongation of the C2-alkyl residue in **1-A** up to an n-heptyl chain leads to a change of the pharmacological profile. A further aspect of this SAR study is the significance of the COOH position at the biphenyl moiety in **1-A** and the consequence of an exchange by a carbonitrile or carboxamide group. Of interest is also the relevance of the benzo[d]imidazole core in **1-A**, which we exchanged by a 2,3-dihydrobenzo[d]thiazole or 1*H*-indole.

The novel compounds were characterized in a PPAR γ differentiation assay using 3T3-L1 cells and in a PPAR γ transactivation assay using transiently transfected COS-7 cells, both established models to assess intracellular PPAR γ activation. Further, we performed a crystal violet chemosensitivity assay in PPAR γ -negative COS-7 and LNCaP prostate cancer cells expressing PPAR γ to evaluate a possible cancer cell line specific PPAR γ -mediated cytotoxic effect. The binding mode of the new compounds has been analyzed in 3D pharmacophore-driven docking experiments.

2. Results and discussion

2.1. Synthesis

For the synthesis of the 4'-((2-propyl-1*H*-benzo[d]imidazol-1-yl)methyl)-[1,1'-biphenyl]-2/3/4-carboxylic acid derivatives **1-A**

(2-COOH), **1-D** (3-COOH), and **1-E** (4-COOH), the respective COOMe-substituted 4-(bromomethyl)-1,1'-biphenyl (**3a-3c**) was reacted with the 2-propyl-1*H*-benzo[d]imidazole **5a** and NaH in DMF giving the 1-([1,1'-biphenyl]-4-ylmethyl)-2-propyl-1*H*-benzo[d]imidazoles **4a-4c**, which were subsequently ester cleaved under basic conditions giving **1-A**, **1-D**, and **1-E** (Scheme 1).

The synthons **3a-3c** are available in a palladium-catalyzed Suzuki-Miyaura coupling of p-tolylboronic acid with either 2-, 3-, or 4-bromobenzoic acid followed by esterification with methanol/H₂SO₄ and halogenation of the methyl group with N-bromosuccinimide (NBS) and benzoylperoxid (BPO) in a Wohl-Ziegler reaction (Scheme 1) [28–30].

The C2-substituted benzo[d]imidazoles **5a-5d** were obtained by a modified Phillips-Ladenburg benzimidazole synthesis [31,32], in which the ortho-phenylenediamine was reacted with the respective acylchloride to the *N,N'*-1,2-phenylenebisalkanoylamids, which then built the benzo[d]imidazoles upon elimination of a carboxylic acid. In the next step, **5a-5d**, respectively, were *N1*-alkylated with 4'-(bromomethyl)-[1,1'-biphenyl]-2-carbonitrile and NaH in DMF (Scheme 2).

The 4'-((2-alkyl-1*H*-benzo[d]imidazol-1-yl)methyl)-[1,1'-biphenyl]-2-carbamides **1-B**, **2-B**, **2-D**, and **2-F** and the respective carboxylic acids **1-A**, **2-A**, **2-C**, and **2-E** were obtained in successive base catalyzed hydrolyses starting from the 4'-((2-alkyl-1*H*-benzo[d]imidazol-1-yl)methyl)-[1,1'-biphenyl]-2-carbonitriles **1-C**, **6b-6d** (Scheme 2). The carbonitrile and the carbamides represent very stable educts, why the yields of the respective products are very low, although very drastic conditions were used (KOH (30%), methanol, reflux, 14d).

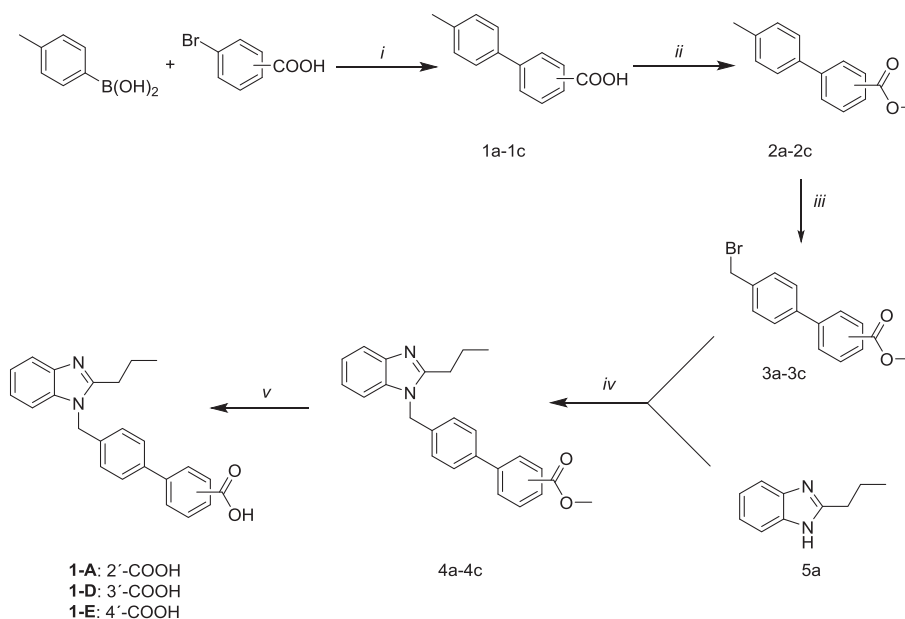
In the first step of the synthesis of the 2-propyl-2,3-dihydrobenzo[d]thiazole **7** (Scheme 3), butyraldehyde was condensed with 2-aminobenzenethiol to a Schiff base, which was not isolated. After addition of methanol and stirring for 0.5 h at RT, cyclization takes place and the product **7** can be isolated in high yields. The *N*-alkylation was performed with 4'-(bromomethyl)-[1,1'-biphenyl]-2-carbonitrile as described above.

As C2 represents a stereo center in **8** and N1 becomes asymmetric due to alkylation, a mixture of two diastereomeric forms in a ratio of 5.5:4.5 were obtained (determined by ¹H-NMR spectroscopy). Fractional crystallization allowed only an enrichment of one diastereomer (7:3) but no separation. Nevertheless, the signals in the NMR-spectra could be assigned to both compounds (see experimental part).

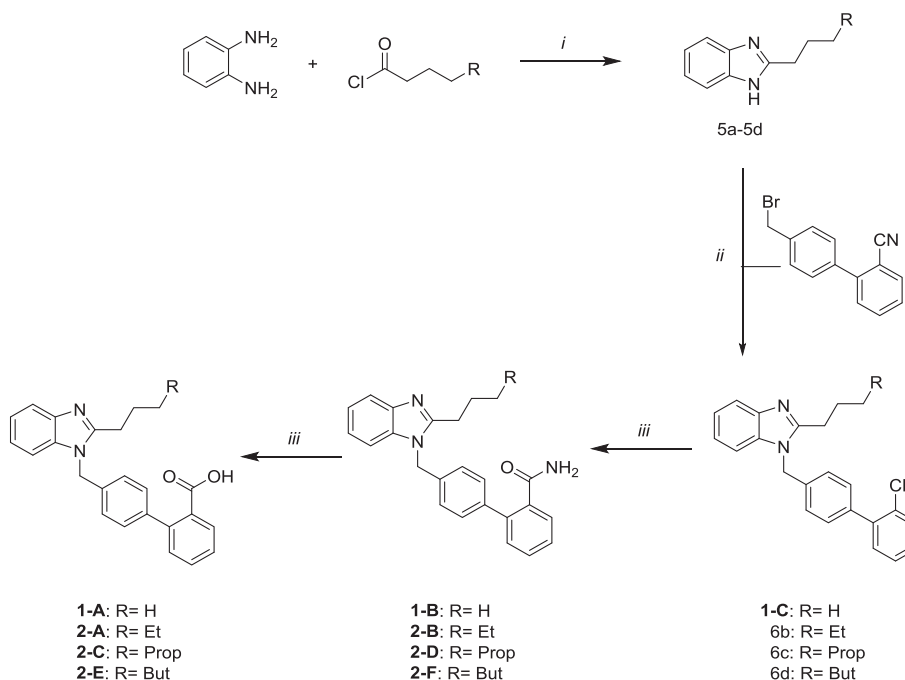
The diastereomeric mixture was then hydrolyzed to the carbamide **3-B** and carboxylic acid **3-A**. No further attempts were made to separate the isomers and the mixtures were submitted to the *in vitro* testing.

For the synthesis of the 1*H*-indole derivatives, an intramolecular Wittig reaction was chosen, which includes three consecutive reactions [33,34]. 2-Aminobenzyl alcohol and triphenylphosphine hydrobromide were dissolved in acetonitrile and heated to reflux. The resulting 2-aminobenzyltriphenylphosphonium bromide **9** was isolated and reacted with butyryl chloride to the carbamide **10**. 2-Butyramidobenzyltriphenylphosphonium bromide **10** was then treated with potassium-*tert*-butylat in toluol. The resulting ylide reacted with the carbonyl C-atom to a phosphor betaine and after elimination of triphenylphosphine oxide, the 2-propyl-1*H*-indole **11** was built (Scheme 4). The subsequent alkylation with 4'-(bromomethyl)-[1,1'-biphenyl]-2-carbonitrile (\rightarrow **3-E**) and hydrolysis to the carbamide **3-D** and carboxylic acid **3-C** was the same as described above.

All compounds were characterized by ¹H-NMR spectroscopy and mass spectrometry and final products, which are evaluated *in vitro* for biological activity, additionally by elemental analysis.



Scheme 1. Synthesis of 4'-((2-propyl-1H-benzo[d]imidazol-1-yl)methyl)-[1,1'-biphenyl]-2/3/4-carboxylic acid derivatives. i) KOH, Pd(OAc)₂, H₂O, RT; ii) H₂SO₄, methanol, ΔT, 5 h; iii) NBS, BPO, CCl₄, ΔT, 4 h; iv) NaH, DMF abs., RT; v) NaOH, methanol, ΔT, 12 h.



Scheme 2. Synthesis of 1-([1,1'-biphenyl]-4-ylmethyl)-2-alkyl-1H-benzo[d]imidazole derivatives. i) ΔT, 3 h; ii) NaH, DMF abs., RT; iii) KOH (30%) methanol, ΔT, 14d.

2.2. In vitro SAR studies

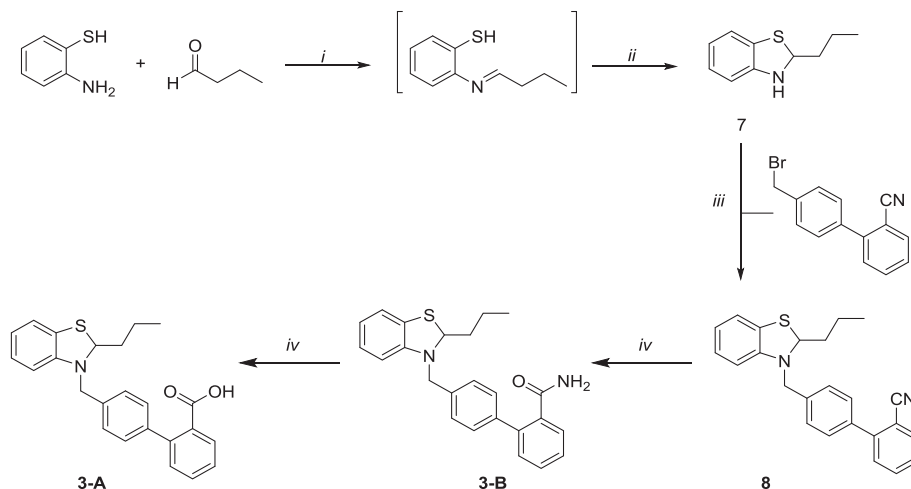
All compounds were characterized in terms of PPAR γ activation in a cell-based dual luciferase transactivation assay (Fig. 1).

The full PPAR γ agonist pioglitazone was used as internal reference and its maximum PPAR γ activation was set as 100%. Table 1 lists the EC₅₀ values and the intrinsic activity (percentage of pioglitazone's activation) at the highest concentration used.

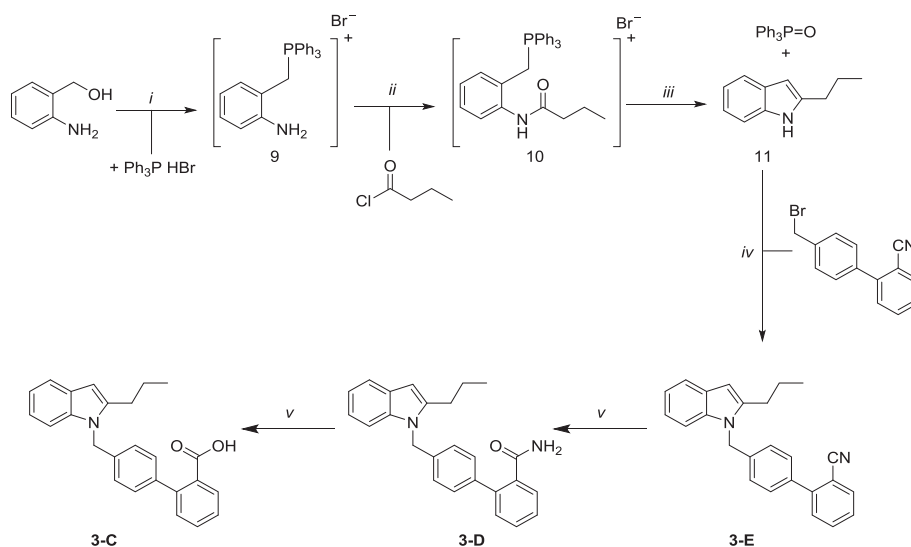
One point of interest is the 2-COOH group at the biphenyl moiety, which can be exchanged by a bioisosteric tetrazole without changing the activity [24]. It is well known that the carboxylate is

involved in the LBD binding via H-bridges. Therefore, we studied the influence of an exchange of the carboxyl group by an carbamide or carbonitrile and a shift of the COOH group from position 2 to the 3/4-position on potency and pharmacological profile of the respective compound.

As depicted in Fig. 1a and b telmisartan, **1-A** (2-COOH) and **1-C** (2-CN) show identical concentration-activity curves representing partial agonists with a maximum activation of about 50% (telmisartan: EC₅₀ = 4.71 μ M, A_{max} = 50.9%; **1-A**: EC₅₀ = 4.17 μ M, A_{max} = 49.6%; **1-C**: EC₅₀ = 5.01 μ M, A_{max} = 51.3%). Interestingly, the carbamide **1-B** shows reduced partial agonism (A_{max} = 21.1%) but



Scheme 3. Synthesis of 3-([1,1'-biphenyl]-4-ylmethyl)-2-propyl-2,3-dihydrobenzo[d]thiazole derivatives. i) RT, 0.5 h; ii) methanol abs., RT, 0.5 h; iii) NaH, DMF, RT; iv) KOH (30% methanol, ΔT , 14d.



Scheme 4. Synthesis of 1-([1,1'-biphenyl]-4-ylmethyl)-2-propyl-1H-indole derivatives. i) acetonitrile, ΔT 6 h; ii) CH_2Cl_2 , ΔT , 3.5 h; iii) t-BuOK, toluol, ΔT , 15 min; iv) NaH, DMF abs., RT; v) KOH (30%) methanol, ΔT , 14d.

slightly increased potency ($\text{EC}_{50} = 3.15 \mu\text{M}$).

The shift of the carboxylic acid from the ortho- to the meta-position does not change the pharmacological profile (**1-D**: $\text{EC}_{50} = 6.24 \mu\text{M}$, $A_{\text{max}} = 44.7\%$). However, both potency ($\text{EC}_{50} = 1.88 \mu\text{M}$) and maximum activity ($A_{\text{max}} = 84.1\%$) increased by shifting the carboxylic acid to the para-position (Fig. 1c). Compound **1-E** represents now a very potent full agonist.

The alkyl chain at position 2 at the benzo[d]imidazole core influences both, the pharmacological profile and the potency. We could already show that the potency reaches a maximum if the benzo[d]imidazole bears a propyl or butyl chain. Furthermore, the efficacy can be increased if a benzyl or a phenethyl moiety is introduced at C2 [27]. In case of a 4-chlorobenzyl residue the pharmacological profile changed from a partial agonist to that of a full agonist. In continuation of this study, we elucidate if the successive elongation of the C2-alkyl residue in **1-A** up to an n-heptyl chain leads to similar effects.

The potency strongly increases in the range: **1-A** (propyl; $\text{EC}_{50} = 4.17 \mu\text{M}$) < **2-A** (pentyl; $\text{EC}_{50} = 0.40 \mu\text{M}$) < **2-C** (hexyl;

$\text{EC}_{50} = 0.21 \mu\text{M}$) < **2-E** (heptyl; $\text{EC}_{50} = 0.17 \mu\text{M}$). All compounds with an elongated alkyl chain are more potent agonists than telmisartan ($\text{EC}_{50} = 4.71 \mu\text{M}$) and comparable to pioglitazone ($\text{EC}_{50} = 0.32 \mu\text{M}$). Parallely, the pharmacological profile changed from that of a partial agonist to that of a full agonist: **1-A** ($A_{\text{max}} = 49.6\%$) = **2-A** ($A_{\text{max}} = 55.4\%$) < **2-C** ($A_{\text{max}} = 75.0\%$) < **2-E** ($A_{\text{max}} = 82.5\%$) (Fig. 1d-f).

The influence of a longer alkyl chain at C2 on the activity of carbamide derivatives is not as significant. **1-B** (propyl; $\text{EC}_{50} = 3.15 \mu\text{M}$, $A_{\text{max}} = 21.1\%$), **2-B** (pentyl; $\text{EC}_{50} = 3.90 \mu\text{M}$, $A_{\text{max}} = 16.2\%$) and **2-D** (hexyl; $\text{EC}_{50} = 3.06 \mu\text{M}$, $A_{\text{max}} = 37.8\%$) show nearly the same results in the transactivation assay. Only the heptyl derivative **2-F** possesses a higher potency ($\text{EC}_{50} = 0.84 \mu\text{M}$) with a comparable maximum activation of $A_{\text{max}} = 32.8\%$.

In the third class of compounds (**3-A** to **3-E**), the necessity of the benzo[d]imidazole for biological activity of the derivatives was studied. If the core in **1-A** is exchanged by a 2,3-dihydrobenzo[d]thiazole, the potency strongly increased: **3-A** shows an $\text{EC}_{50} = 1.05 \mu\text{M}$ with an intrinsic activity of $A_{\text{max}} = 57.4\%$. In the case

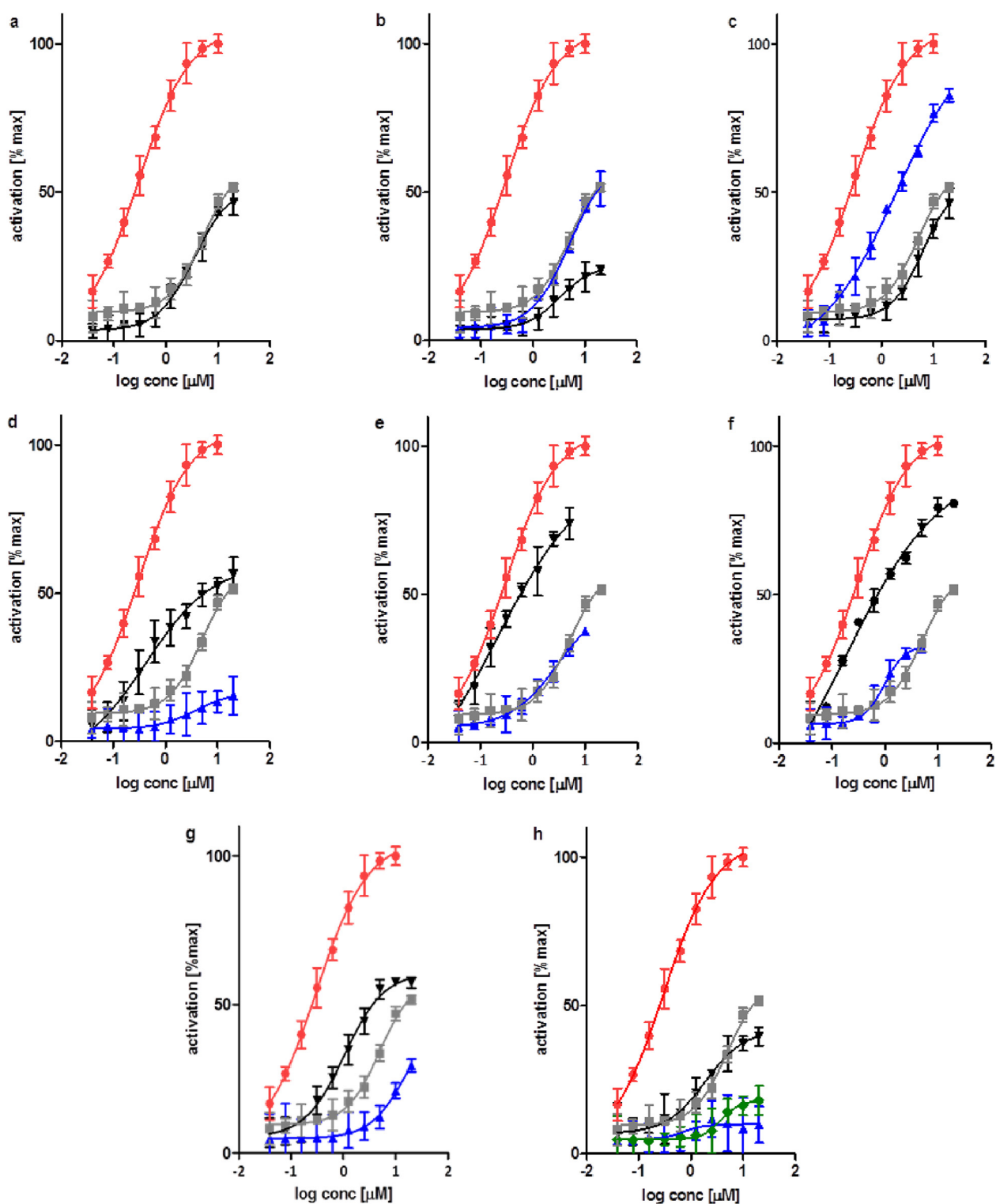


Fig. 1. PPAR γ activation measured in a luciferase transactivation assay. COS-7 cells were transiently transfected with the pGal4-hPPAR γ DEF and pGal5-Tk-pGL3 followed by stimulation with pioglitazone (\bullet), or telmisartan (\blacksquare), or the synthesized compounds a) essential scaffold **1-A** (\blacktriangledown) b) **1-B** (\blacktriangledown), **1-C** (\blacktriangle); c) **1-D** (\blacktriangledown), **1-E** (\blacktriangle); d) **2-A** (\blacktriangledown), **2-B** (\blacktriangle); e) **2-C** (\blacktriangledown), **2-D** (\blacktriangle); f) **2-E** (\blacktriangledown), **2-F** (\blacktriangle); g) **3-A** (\blacktriangledown), **3-B** (\blacktriangle); h) **3-C** (\blacktriangledown), **3-D** (\blacktriangle), **3-E** (\blacklozenge) in a concentration-dependent manner. Firefly-luciferase was measured after 42 h and normalized with the activity of the co-transfected pCMV-Renilla. Data points represent mean \pm SD of ≥ 3 independent experiments with threefold determination.

of **3-B** (carbamide derivative) only a marginal transactivation ($A_{\max} = 33.1\%$) is determined at higher concentrations ($20 \mu\text{M}$) and its curve progression does not allow a statement about the pharmacological profile (Fig. 1g).

As depicted in Fig. 1h, the data of the 1*H*-indole derivatives **3-C**, **3-D** and **3-E** give sigmoid concentration-activation curves. The maximum intrinsic activation is in each case lower than 50%: **3-C** ($A_{\max} = 40.0\%$) > **3-E** ($A_{\max} = 21.7\%$) > **3-D** ($A_{\max} = 11.0\%$). From

Table 1

EC₅₀ values and maximum intrinsic activity [A_{max}] determined in the luciferase transactivation assay using the hPPAR γ -LBD.

Compound	EC ₅₀ [μ M] ^{a,c}	A _{max} [%max] ^{b,c}
Pioglitazone	0.32 \pm 0.08	100
Telmisartan	4.71 \pm 0.26	50.9 \pm 2.1
1-A	4.17 \pm 0.28	49.6 \pm 2.3
1-B	3.15 \pm 0.26	21.1 \pm 2.4
1-C	5.01 \pm 0.22	51.3 \pm 3.6
1-D	6.24 \pm 0.17	44.7 \pm 3.4
1-E	1.88 \pm 0.10	84.1 \pm 3.8
2-A	0.40 \pm 0.03	55.4 \pm 3.0
2-B	3.90 \pm 0.07	16.2 \pm 1.0
2-C	0.21 \pm 0.02	75.0 \pm 0.5
2-D	3.06 \pm 0.09	37.8 \pm 0.7
2-E	0.17 \pm 0.02	82.5 \pm 3.0
2-F	0.84 \pm 0.06	32.8 \pm 1.2
3-A	1.05 \pm 0.07	57.4 \pm 1.1
3-B	n.d.	33.1 \pm 5.0
3-C	1.86 \pm 0.09	40.0 \pm 1.7
3-D	n.d.	11.0 \pm 1.7
3-E	8.03 \pm 0.25	21.7 \pm 2.1

^a EC₅₀ values were calculated by means of concentration-PPAR γ activation-curves (Fig. 1).

^b The maximum activation [A_{max}] indicates the highest reached response triggered by the compounds and is shown in relation to pioglitazone (100%).

^c Data values represent mean \pm SD of three independent experiments.

these curves the EC₅₀ values can be calculated showing that **3-C** (EC₅₀ = 1.86 μ M) is a more potent partial agonist than **1-A**. The intrinsic activity and the potency of **3-E** (EC₅₀ = 8.03 μ M) is strongly decreased compared to **1-A** and from the curve of **3-D** an EC₅₀ value cannot be calculated beyond doubt.

In the next step, we studied the relevance of the structural modifications in an adipocyte differentiation assay. In 3T3-L1 cells, the PPAR γ activation strongly correlates with the degree of differentiation, which was analyzed by Oil-Red O staining. Telmisartan and pioglitazone were used as positive controls and DMSO as vehicle. Results are shown in Fig. 2. Pioglitazone as full agonist induced a triglyceride accumulation (TG accumulation) up to 4-fold compared to the vehicle. The partial agonist telmisartan was nearly inactive at a concentration of 1 μ M and showed an about 2-fold TG accumulation at 10 μ M (Fig. 2). Compounds **1-A**, **1-B**, and **1-C** with COOH, CONH₂ and CN substituents at 2-position were comparably active, whereas the shift of the carboxylic acid from the ortho- (**1-A** (10 μ M): 3.2-fold) to the meta- (**1-D** (10 μ M): 2.5-fold) and finally to the para-position (**1-E** (10 μ M): 1.2-fold) reduced strongly the TG-accumulation.

In the second class of compounds, the 2-carbamide-substituted

compounds caused a distinctly reduced TG accumulation compared to the COOH derivatives especially at 1 μ M. The latter (**2-A**, **2-C** and **2-E**), which proved to be partial or strong partial agonists in the PPAR γ transactivation assay, induced differentiation at both tested concentrations (1 μ M and 10 μ M) to approximately the same extent as measured for the full agonist pioglitazone. It should be noted that all derivatives are more potent than telmisartan.

The general trends were also determined in the third class of compounds: 2-COOH (**3-C**) > 2-CONH₂ (**3-D**) > 2-CN (**3-E**); 2-COOH derivatives (**3-A**, **3-C**) reached at 10 μ M nearly the effects of pioglitazone (>3-fold TG accumulation). These results further imply that the activity in the adipocyte differentiation assay is not dependent on the used heterocyclic core. Furthermore, there is no correlation with the transactivation assay.

As multiple studies established an association between full PPAR γ agonism and adipocyte differentiation *in vitro* and weight gain *in vivo*, compound **1-E** is certainly outstanding in this SAR study due to its non-adipogenic effect although it represents a potent full agonist.

During the last years an increasing number of studies were published showing the antitumor potency of PPAR γ agonists and antagonists *in vitro* and *in vivo*. The cytotoxicities are discussed to be PPAR γ -dependent or -independent. Therefore, we studied the growth inhibitory effects of the class 1–3 agonists in the androgen-dependent LNCaP prostate cancer cell line expressing PPAR γ [35] as well as in healthy COS-7 cells, which were used as transfection vector in the luciferase transactivation assay.

The test concentration (50 μ M) was chosen according to previously published studies with telmisartan in different cell lines of the urogenital system [23].

The results depicted in Fig. 3 indicate a growth inhibitory effect of about 55.8% in LNCaP cells for pioglitazone, while it was inactive in COS-7 cells. On the other hand telmisartan did not influence the growth of both cell lines.

Among the class 1 compounds a clear structure-activity relationship was observed. The cell growth was reduced in the series **1-A** (2-COOH: inactive) < **1-B** (CONH₂: 33.0%) < **1-C** (2-CN: 61.9%) The shift of the carboxylic acid did not influence the effects of the compounds (**1-D**, **1-E**) on the growth of both cell lines.

Derivatives out of class 2 exerted effects on the cells dependent on the length of the C2-alkyl chain and the 2-substituent. While all 2-COOH bearing compounds were inactive, **2-B**, **2-D**, and **2-F** showed pronounced antiproliferative effects with a slight preference for COS-7 cells. **2-D** was the most active derivative with a reduced cell growth of 78.5% in LNCaP cells and 92.8% in COS-7 cells. The dihydrobenzo[d]thiazole derivatives demonstrated a comparable pharmacological profile (**3-A** inactive; **3-B** inhibition of

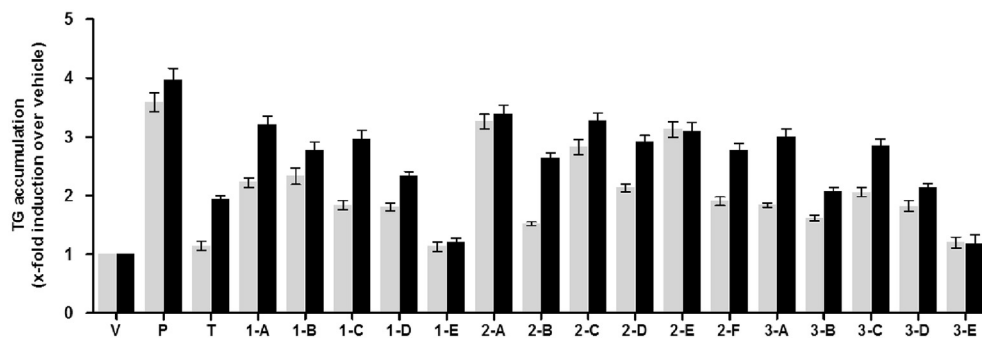


Fig. 2. Compound screening in an adipocyte differentiation assay. 3T3-L1 cells were differentiated for 9 days with the indicated compounds at 1 μ M (■) and 10 μ M (■). Telmisartan (T) and pioglitazone (P) served as positive controls and DMSO (V) as vehicle. Cells were stained with Oil-Red O and the dye was subsequently extracted with 80% isopropanol. Intracellular triglyceride accumulation was determined by measuring absorbance of extraction solution at 515 nm. Values were set in ratio to the vehicle value. Data points represent mean \pm SD of three independent experiments.

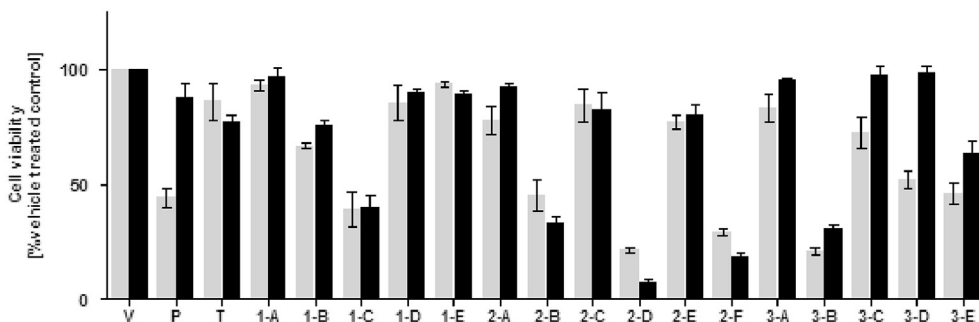


Fig. 3. Cytotoxicity screening of the respective compounds in an *in vitro* chemosensitivity assay. LNCaP (■) and COS-7 cells (■) were treated with the compounds; telmisartan (T) or pioglitazone (P) at a concentration of 50 μ M. Cell biomass was determined after 72 h via crystal violet staining and subsequent measurement of absorbance at 595 nm. Cell biomass is represented as % of cell biomass of vehicle (V) treated control.

79.0% in LNCaP cells and 69.2% in COS-7 cells). Interestingly, the influence of 1*H*-indole derivatives against LNCaP cells was higher than against COS-7 cells. While only **3-E** reduced the growth of COS-7 cells (by 36.8%) **3-C**, **3-D** and **3-E** were cytotoxic on the LNCaP cell line (growth reduction 27.4–54.1%).

Based on these results it seems to be very unlikely that the active compounds possess a PPAR γ -mediated mode of action. Only the 1*H*-indole derivatives and pioglitazone were more active on PPAR γ expressing LNCaP cells than on COS-7 cells.

2.3. Docking studies to predict PPAR γ binding

In order to investigate the binding mode of the new compound series to PPAR γ , molecular modeling studies were performed. The high-resolution structure of PPAR γ co-crystallized with telmisartan and the coactivator peptide from steroid receptor coactivator-1 (PDB code 3VN2 [36]) was selected to investigate potential binding modes of the compounds by computational docking experiments.

First, we performed a 3D pharmacophore analysis to identify key interactions formed by telmisartan (Fig. 4): the highly hydrophobic receptor binding site is characterized by a Y-shaped form that can be subdivided into the arms I, II and III [37–39]. In the aforementioned crystal structure, telmisartan adopts a U-shaped conformation around Cys285 [36], which adjusts our previous hypothesis on telmisartan binding [25]: the central benzo[*d*]imidazole ring occupies arm I, and its N3' nitrogen forms a hydrogen bond with the hydroxyl group of Tyr473 that is part of helix 12, representing the only observed H-bond formed by the ligand. The

propyl moiety fills an extension of the arm I, which is formed by pushing out the side chain of His323 in comparison to its position in other crystal structures [25]. Hydrophobic contacts are formed with Tyr473, Ile472, Tyr327 and Ile326. Additionally, π -stacking interactions are formed by the distal benzo[*d*]imidazole ring and Phe363 in arm I. The biphenyl moiety is located in arms II and III and forms hydrophobic contacts with Met364, Ile341, Val339 and Ile326. The carboxylate is located in direction to Arg288 but not close enough to form H-bonds to residues of helix 2.

Next, the synthesized compounds were docked into the same crystal structure in order to identify a potential binding mode. Binding poses were selected according to their similarity to the telmisartan binding mode putting special emphasis on the hydrophobic contacts formed with the arm I extension resulting from the movement of His323. This resulted in the predicted binding modes discussed below.

Binding conformations and rationalization of structure-activity relationship derived from docking experiments

Compounds **1-A**, **1-B**, **1-C**, and **1-D** show an orientation of the annelated ring system comparable to telmisartan. The propyl moiety in **1-A** is located in the extension of arm I created by the His323 movement and forms hydrophobic contacts with Val322, Ile472, Leu469, Val293 and Ile326 (Fig. 5A). The position of the benzo[*d*]imidazole is stabilized by an H-bond formed by the N3'-nitrogen and the hydroxyl group of Tyr473. The biphenyl moiety is located in arms II and III and in hydrophobic contacts with Leu330, Ile341, Ile326 and Met364. The carboxylate in **1-A** is bound to Arg288 by an H-bridge and a negative charge interaction (Fig. 5A). In the case of **1-B** the carboxylate group is exchanged by a

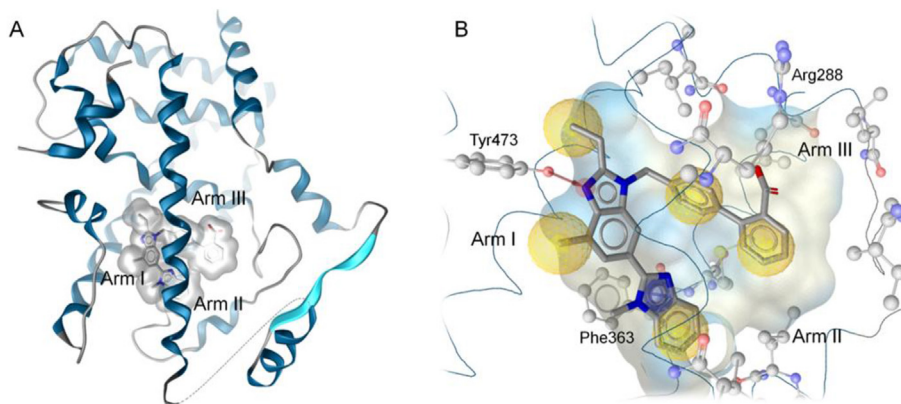


Fig. 4. Binding mode of telmisartan to PPAR γ . A) PPAR γ co-crystallized with telmisartan. The receptor is shown in blue, the ligand in stick mode. Its van der Waals surface is depicted in grey. B) Telmisartan in the PPAR γ binding site. Key interactions are marked in color code: yellow spheres – hydrophobic contacts, blue ring – π -stacking, red arrow – H-bond acceptor. (For interpretation of the references to colour in this figure legend, the reader is referred to the web version of this article.)

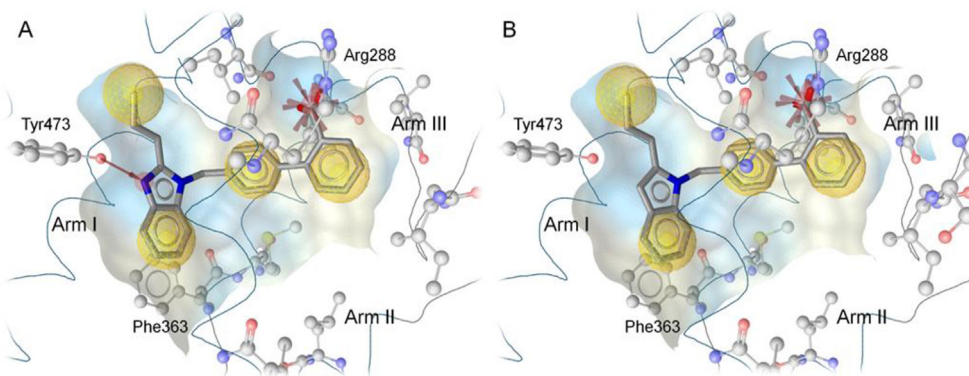


Fig. 5. Impact of the substitution of the benzo[*d*]imidazole through an *1H*-indole. A) 3D view of the binding mode of compound **1-A**. One H-bond between the benzo[*d*]imidazole moiety and Tyr473 is depicted as a red arrow, the charge interaction with Arg288 as a red star. Hydrophobic contacts are shown as yellow spheres. B) Binding mode predicted for compound **3-C** is analogous to the one for **1-A**. However, the stabilizing H-bond to Tyr473 is missing. (For interpretation of the references to colour in this figure legend, the reader is referred to the web version of this article.)

carbamide moiety, thus the negative charge interaction between the ligand and Arg288 is missing. Furthermore, the charge distribution in the carbamide seems to cause a repulsion to Arg288 which could be the reason for the decrease in intrinsic activity (lowering of A_{\max}). Compound **1-C** bearing a 2-carbonitrile group possesses the same pharmacological profile as **1-A**. The stabilization through the H-bond from Tyr473 to the N3'-nitrogen of the heterocycle seems, therefore, to be sufficient to stabilize the binding in the LBD and maintain the intrinsic activity.

Alternatively, agonists can also activate the receptor through binding of the 2-carboxylate group to Arg288. The *1H*-indole derivative **3-C** is located nearly identically to **1-A** in the LBD (Fig. 5B) without having contact to Tyr473. This missing link leads only to a marginal reduction of the intrinsic activity (A_{\max} : 49.6% → 40.0%). However, if both key interactions are missing, e.g. by the exchange of the carboxylate by a carbamide (**3-D**), the binding to Arg288 is impossible leading to a nearly complete loss of activity (A_{\max} = 11.0%).

Surprisingly, the shift of the 2-carboxylate to the 4-position (**1-A** → **1-E**) causes the ligand to flip and the propyl substituent is now located in the binding site of arm I (Fig. 6A). In this case the benzene part of the benzo[*d*]imidazole ring is embedded in the aperture close to His323. The biphenyl moiety is slightly shifted and the carboxylate forms two H-bonds to the backbone nitrogens of Ser342 and Glu343, which presumably causes an increased stabilization of helix 3 and the β -sheet region in our model. This orientation leads to an increase in potency (EC_{50} = 1.88 μ M) and

intrinsic activity (A_{\max} = 84.1%). The pharmacological profile is now that of a full agonist.

Interestingly, the elongation of the C2-propyl chain in **1-A** to pentyl (**2-A**), hexyl (**2-C**), or heptyl (**2-E**) forces the benzo[*d*]imidazole in a binding mode comparable to **1-E** and in opposite direction as in telmisartan or **1-A**. The long alkyl chains do not fit the cavity extension close to His323 (Fig. 7). The biphenyl moiety of the compounds is oriented in arms II and III and the binding is stabilized in the case of the carboxylated compounds by the charge interaction to Arg288.

The intrinsic activity (49.6% for propyl (**1-A**), 55.4% for pentyl (**2-A**), 75.0% for hexyl (**2-C**) and 82.5% for heptyl (**2-E**)) as well as the potency (EC_{50} (**1-A**) = 4.19 μ M; EC_{50} (**2-A**) = 0.40 μ M; EC_{50} (**2-C**) = 0.21 μ M; EC_{50} (**2-E**) = 0.17 μ M) of the 2-carboxylate containing compounds increase with longer alkyl groups. **2-E** is a very potent full agonist. Its long heptyl chain reaches into arm II (Fig. 7B) and forms multiple hydrophobic contacts with residues as Ile281, Leu356 and Leu353 what further stabilizes the activated conformation of the receptor.

The lack of the Arg288 interaction in the compounds with a carbamide substituent (**2-B**, **2-D** and **2-F**) causes a decrease in intrinsic activity and potency, showing that it is essential for the orientation and stabilization of these ligands and functions as an anchoring point in the binding site.

The exchange of the benzo[*d*]imidazole core through a 2,3-dihydrobenzo[*d*]thiazole ring causes a moderate increase in activity for **3-A** compared to **1-A**. In the predicted binding mode, the 2,3-

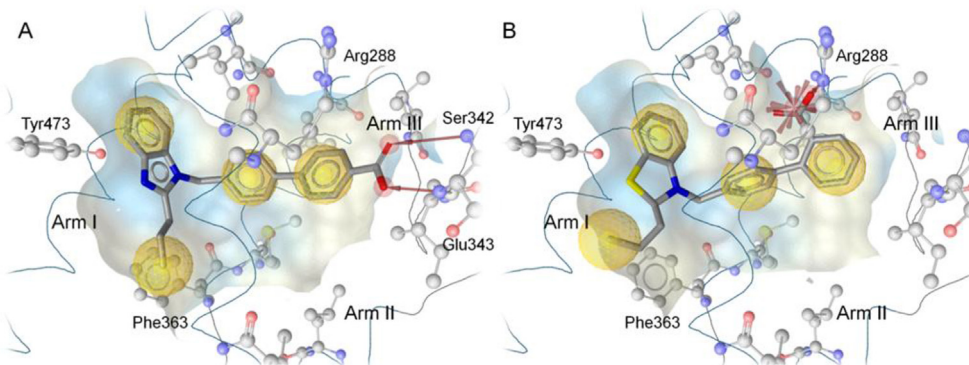


Fig. 6. Binding modes of compounds **1-E** and **3-A** that share the flipped ring orientation. A) Predicted binding mode for compound **1-E** forming two H-bonds to residues Ser342 and Glu343 (depicted as red arrows) that stabilize the binding mode. B) 3D view of the binding pose of compound **3-A**. The ligand is anchored by the charge interaction with Arg288. (For interpretation of the references to colour in this figure legend, the reader is referred to the web version of this article.)

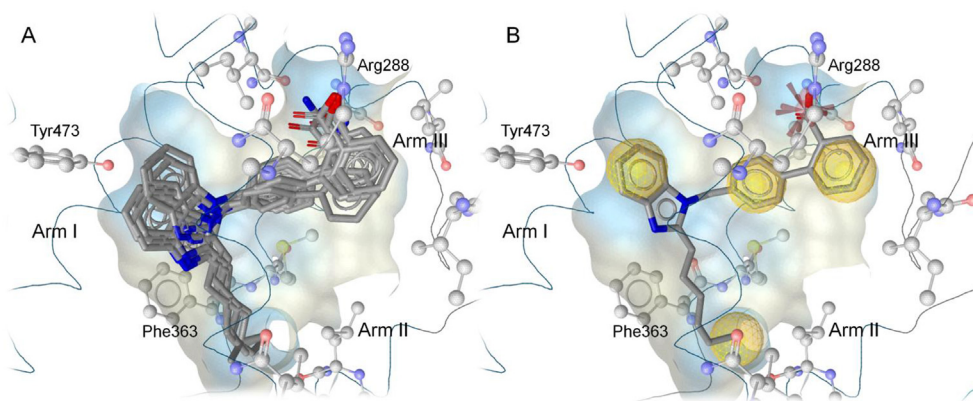


Fig. 7. Overview on the binding mode of the compounds with varying alkyl-chain length. A) Superimposed compounds **2-A** to **2-F** that show the flipped orientation of the benzo[d]imidazole in the binding pocket B) Binding mode of compound **2-E**. The long heptyl chain forms multiple hydrophobic contacts with residues as Ile281, Leu356 and Leu353.

dihydrobenzo[d]thiazole compound is comparably oriented as compounds **2-A** to **2-F** (Fig. 6B). The flexibility of the ring system makes it possible for the benzene moiety of the heterocycle to be deeply embedded into the cavity region close to His323, which could explain the enhanced activity. Interestingly, also in this series the exchange of the carboxylate by a carbamide (**3-B**) causes a loss of activity and potency showing again that the charge interaction between the carboxylate and Arg288 is necessary to stabilize this binding pose.

3. Conclusions

Extending our studies on PPAR γ agonists, new derivatives of the lead structure **1-A** have been synthesized with the following modifications: elongation of the alkyl chain at position 2 of the benzo[d]imidazole, exchange or shift of the carboxylic acid residue at the biphenyl moiety and exchange of the central benzo[d]imidazole.

In pharmacological *in vitro* studies most of the new compounds demonstrated potent PPAR γ activation (EC_{50} values between 0.17 and 8.03 μ M) with distinct pharmacological profiles ranging from weak partial agonists to full agonists. Interestingly, data from the PPAR γ activation assay correlate only partially with those from the functional preadipocyte differentiation assay. For example, the full agonist **1-E** induced TG accumulation only to a very low extent. Also in the cytotoxicity assay using PPAR γ positive prostate cancer cells no thorough correlation with the results from the PPAR γ transactivation assay was observed indicating that occurring cytotoxic effects are likely to be independent from PPAR γ .

In 3D pharmacophore-driven docking experiments, we demonstrated that in the LBD of the PPAR γ two anchoring points (Tyr473 and Arg288) through which an agonist can activate the receptor exists. Either the N3'-nitrogen of the 1-([1,1'-biphenyl]-4-ylmethyl)-1H-benzo[d]imidazole core (H-bridge with the Tyr473) or an H-bridge and a negative charge interaction from the 2-carboxylate to Arg288 must be present to achieve the pharmacological profile of a partial agonist (binding mode 1).

If the carboxylate is shifted to the 4-position or the C2-alkyl chain is elongated, the orientation of the benzo[d]imidazole is turned by 180° and the compounds have the profile of full agonists (binding mode 2). It is very likely, that the 1-([1,1'-biphenyl]-4-ylmethyl)-1H-benzo[d]imidazole derivatives can bind to the LBD in both conformations. However, the longer the C2-chain the higher is the proportion of binding mode 2 which goes along with lower EC_{50} values and higher maximum activation. Furthermore,

with Ser342 and Glu343 further anchoring points for full agonists were identified.

4. Experimental section

4.1. General material and methods

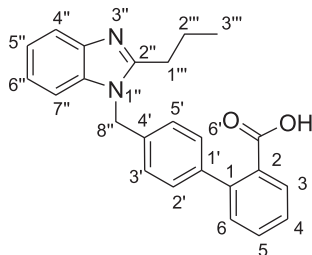
All reagents and solvents were purchased from Acros Organics, Sigma-Aldrich, Alfa Aesar or Merck. All reactions were monitored by TLC, performed on silica gel plates 60 F254 (Merck, Darmstadt/Germany). Visualization on TLC was achieved by UV light. Column chromatography was performed with Merck silica gel 60H, grain size <0.063 mm, 230 mesh ASTM (Darmstadt/Germany). Melting points were determined on a B 545 Büchi (Flawil/Schweiz) capillary melting point apparatus. 1 H-NMR spectra were obtained with an Avance DPX-400 spectrometer (Bruker, Karlsruhe/Germany) at 400 MHz using TMS as an internal standard. 13 C-NMR spectra were measured with a Gemini 2000 NMR spectrometer (Varian, Palo Alto/USA) at 50 MHz using TMS as an internal standard. Elemental analyses were carried out at the Microlaboratory of the Freie Universität Berlin with a Vario EL elemental analyzer (Elementar, Hanau/Germany). Mass spectra were obtained with an Orbitrap Elite ESI mass spectrometer (Thermo Fisher, Waltham/USA). The analytical results are within 0.4% of theoretical values, indicating that the purity of all tested compounds was higher than 95%. EIMS spectra were obtained with a CH-7A-Varian MAT, 70 eV (Melbourne/Australia). Absorbance and luminescence in biological assays were measured with an Enspire Multimode Plate Reader (Perkin-Elmer, Life Sciences, Brunn/Austria).

4.2. Chemistry

4.2.1. General method for the preparation of 4'-((2-propyl-1H-benzo[d]imidazol-1-yl)methyl)-[1,1'-biphenyl]-carboxylic acids

To a stirred solution of the respective methyl 4'-((2-propyl-1H-benzo[d]imidazol-1-yl)methyl)-[1,1'-biphenyl]-carboxylate (0.10 g, 0.26 mmol) in 10 ml of abs. methanol, 0.21 ml of NaOH (10%) (0.52 mmol) were added and heated to reflux for 12 h. After cooling to RT, the mixture was acidified with HCl and the product was extracted with methylene chloride. After drying over Na_2SO_4 , the solvent was removed in vacuo and the crude product was purified by column chromatography on silica gel with methylene chloride/methanol (9:1) and recrystallization from diethyl ether and methanol.

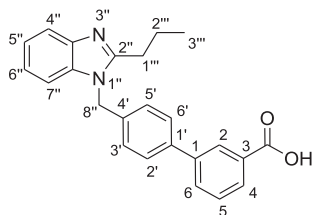
4.2.1.1. 4'-((2-Propyl-1H-benzo[d]imidazol-1-yl)methyl)-[1,1'-biphenyl]-2-carboxylic acid (**1-A**).



Colorless crystals; yield 0.08 g (0.22 mmol, 85%); mp 153 °C.

¹H-NMR (400 MHz/DMSO-*d*₆): δ 12.72 (s, 1H, COOH), 7.70 (dd, 1H, H₃), 7.59 (m, 1H, H₄'), 7.54 (ddd, 1H, H₅), 7.50 (m, 1H, H₇''), 7.43 (ddd, 1H, H₄), 7.33 (dd, 1H, H₆), 7.28 (d, ³J = 8.1 Hz, 2H, H₂' + H₆'), 7.17 (m, 2H, H₅' + H₆''), 7.12 (d, ³J = 8.1 Hz, 2H, H₃' + H₅'), 5.53 (s, 2H, CH₂ 8''), 2.84 (t, ³J = 7.4 Hz, 2H, CH₂ 1'''), 1.79 (tq, ³J = 7.4 Hz, 2H, CH₂ 2'''), 0.96 (t, ³J = 7.4 Hz, 3H, CH₃ 3'''). MS: (EI, 170 °C) *m/z* 370.4 (M + 100%); Anal. calcd for C₂₄H₂₂N₂O₂: C 77.81, H 5.99, N 7.56; found: C 78.05, H 6.34, N 7.56.

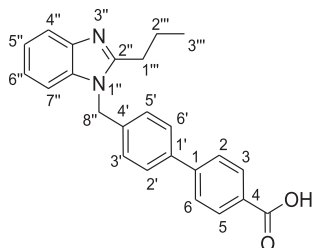
4.2.1.2. 4'-((2-Propyl-1H-benzo[d]imidazol-1-yl)methyl)-[1,1'-biphenyl]-3-carboxylic acid (**1-D**).



Colorless crystals; yield 0.09 g (0.24 mmol, 92%); mp 234 °C.

¹H-NMR (400 MHz/DMSO-*d*₆): δ 13.07 (s, 1H, COOH), 8.14 (dd, 1H, H₂), 7.89 (m, 2H, H₄ + H₆), 7.66 (d, ³J = 8.3 Hz, 2H, H₂' + H₆'), 7.58 (m, 2H, H₅ + H₄''), 7.47 (m, 1H, H₇'), 7.20 (d, 2H, ³J = 8.3 Hz, H₃' + H₅'), 7.16 (m, 2H, H₅' + H₆''), 5.55 (s, 2H, CH₂ 8''), 2.84 (t, ³J = 7.4 Hz, 2H, CH₂ 1'''), 1.78 (tq, ³J = 7.3 Hz, 2H, CH₂ 2'''), 0.96 (t, ³J = 7.3 Hz, 3H, CH₃ 3'''). MS: (EI, 200 °C) *m/z* 370.3 (M + 71%); Anal. calcd for C₂₄H₂₂N₂O₂: C 77.81, H 5.99, N 7.56; found: C 77.79, H 6.00, N 7.57.

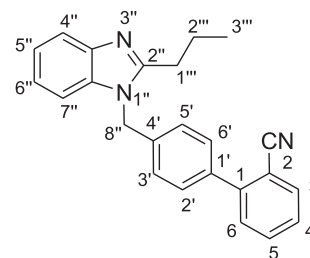
4.2.1.3. 4'-((2-Propyl-1H-benzo[d]imidazol-1-yl)methyl)-[1,1'-biphenyl]-4-carboxylic acid (**1-E**).



Colorless crystals; yield 0.09 g (0.24 mmol, 92%); mp 247 °C.

¹H-NMR (400 MHz/DMSO-*d*₆): δ 12.97 (s, 1H, COOH), 7.99 (d, ³J = 8.4 Hz, 2H, H₂ + H₆), 7.76 (d, ³J = 8.4 Hz, 2H, H₃ + H₅), 7.70 (d, ³J = 8.3 Hz, 2H, H₂' + H₆'), 7.6 (m, 1H, H₄'), 7.47 (m, 1H, H₇''), 7.20 (d, ³J = 8.3 Hz, 2H, H₃' + H₅'), 7.16 (m, 2H, H₅' + H₆''), 5.56 (s, 2H, CH₂ 8''), 2.84 (t, ³J = 7.4 Hz, 2H, CH₂ 1'''), 1.79 (tq, ³J = 7.4 Hz, ³J = 7.3 Hz, 2H, CH₂ 2'''), 0.96 (t, ³J = 7.3 Hz, 3H, CH₃ 3'''). ¹³C-NMR (200 MHz, DMSO-*d*₆) δ 167.65, 155.60, 144.23, 142.95, 138.67, 137.87, 135.84, 130.48, 130.23, 127.87, 127.68, 127.24, 122.27, 121.92, 119.06, 110.69, 46.16, 29.06, 20.89, 14.35. HR-MS: calcd for C₂₄H₂₂N₂O₂ [M + H]⁺: 371.1773; found: 371.1747. MS: (EI, 200 °C) *m/z* 370.3 (M⁺ 61%); Anal. calcd for C₂₄H₂₂N₂O₂: C 77.81, H 5.99, N 7.56; found: C 77.78, H 6.01, N 7.56.

4.2.1.4. 4'-((2-Propyl-1H-benzo[d]imidazol-1-yl)methyl)-[1,1'-biphenyl]-2-carbonitrile (**1-C**). The 1H-benzo[d]imidazole 5a (2.50 mmol) was dissolved in 10 ml of abs. DMF. Sodium hydride (60% dispersion in mineral oil) (0.2 g, 5 mmol) was added with cooling. After the gas formation stopped, 4'-bromomethyl-[1,1'-biphenyl]-2-carbonitrile dissolved in 2 ml of abs. DMF was added dropwise and the solution was stirred for 1 h under cooling in an ice bath and further 2 h at RT. Water was added and after the solution was acidified with HCl, the product was extracted three times with methylene chloride. The combined organic layers were dried over Na₂SO₄ and evaporated to dryness in vacuo. The crude product was purified by column chromatography on silica gel with methylene chloride/methanol (95:5) and recrystallized from diethyl ether/methanol.



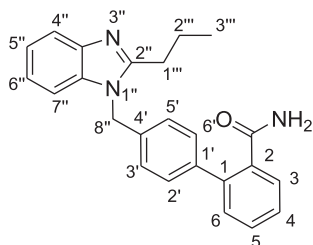
Grey-colored wax-like paste; yield 0.62 g (1.76 mmol, 70%).

¹H-NMR (400 MHz/DMSO-*d*₆): δ 7.93 (d, 1H, H₃), 7.76 (ddd, 1H, H₅), 7.61 (m, 1H, H₄'), 7.57 (m, 2H, H₄ + H₆), 7.55 (d, ³J = 8.3 Hz, 2H, H₂' + H₆'), 7.50 (m, 1H, H₇''), 7.23 (d, ³J = 8.3 Hz, 2H, H₃' + H₅'), 7.17 (m, 2H, H₅' + H₆''), 5.59 (s, 2H, CH₂ 8''), 2.85 (t, ³J = 7.5 Hz, 2H, CH₂ 1'''), 1.78 (tq, ³J = 7.5 Hz, ³J = 7.4 Hz, 2H, CH₂ 2'''), 0.96 (t, ³J = 7.4 Hz, 3H, CH₃ 3'''). MS: (EI, 50 °C) *m/z* 351.3 (M⁺ 67%); Anal. calcd for C₂₄H₂₁N₃: C 82.02, H 6.02, N 11.96; found: C 82.10, H 6.20, N 11.76.

4.2.2. General method for the preparation of C2-substituted 4'-((1H-benzo[d]imidazol-1-yl)methyl)-[1,1'-biphenyl]-2-carbamides and 4'-((1H-benzo[d]imidazol-1-yl)methyl)-[1,1'-biphenyl]-2-carboxylic acids

The respective 4'-((2-alkyl-1H-benzo[d]imidazol-1-yl)methyl)-[1,1'-biphenyl]-2-carbonitrile (1.00 mmol) was dissolved in 15 ml of methanol and combined with 5.61 ml of KOH (30%) (30 mmol). The mixture was heated to reflux for 14d. After cooling to RT, HCl was added until the solution was acidified. Subsequently, the crude product was isolated by extraction with methylene chloride. After drying over Na₂SO₄, the solvent was removed in vacuo and the products were separated by column chromatography on silica gel with methylene chloride/methanol (95:5) and recrystallized from diethyl ether/methanol.

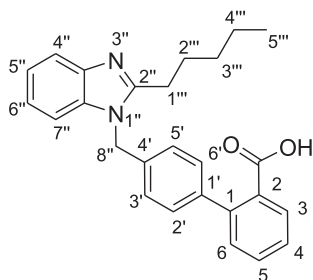
4.2.2.1. 4'-((2-Propyl-1H-benzo[d]imidazol-1-yl)methyl)-[1,1'-biphenyl]-2-carbamide (**1-B**).



Colorless crystals; yield 0.04 g (0.11 mmol, 11%); mp 170 °C.

$^1\text{H-NMR}$ (400 MHz/DMSO- d_6): δ 7.62 (s, 1H, NH), 7.59 (m, 1H, H4''), 7.49 (m, 1H, H7''), 7.44 (ddd, 1H, H4), 7.40 (dd, 1H, H3) 7.39 (ddd, 1H, H5) 7.37 (d, $^3J = 8.3$ Hz, 2H, H2' + H6'), 7.32 (d, 1H, H6), 7.24 (s, 1H, NH), 7.16 (m, 2H, H5'' + H6''), 7.11 (d, $^3J = 8.3$ Hz, 2H, H3' + H5'), 5.52 (s, 2H, CH₂ 8''), 2.84 (t, $^3J = 7.5$ Hz, 2H, CH₂ 1'''), 1.79 (tt, $^3J = 7.5$ Hz, $^3J = 7.4$ Hz, 2H, CH₂ 2'''), 0.97 (t, $^3J = 7.4$ Hz, 3H, CH₃ 3'''). MS: (EI, 200 °C) m/z 369.4 (M^+ 79%); Anal. calcd for C₂₄H₂₃N₃O: C 78.02, H 6.27, N 11.37; found C 78.22, H 6.26, N 11.39.

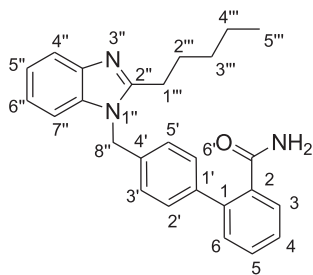
4.2.2.2. 4'-((2-Pentyl-1H-benzo[d]imidazol-1-yl)methyl)-[1,1'-biphenyl]-2-carboxylic acid (**2-A**).



Beige-colored powder; yield 0.08 g (0.20 mmol, 22%); mp 193 °C.

$^1\text{H-NMR}$ (400 MHz/DMSO- d_6): δ 12.73 (s, 1H, COOH), 7.70 (dd, 1H, H3), 7.59 (m, 1H, H4''), 7.54 (ddd, 1H, H5), 7.51 (m, 1H, H7''), 7.43 (ddd, 1H, H4), 7.32 (ddd, 1H, H6), 7.28 (d, 2H, H2' + H6'), 7.17 (m, 2H, H5'' + H6''), 7.12 (d, 2H, H3' + H5'), 5.53 (s, 2H, CH₂ 8''), 2.85 (t, 2H, CH₂ 1'''), 1.74 (tt, 2H, CH₂ 2'''), 1.30 (m, 4H, CH₂ 3'''' + CH₂ 4'''), 0.84 (t, 3H, CH₃ 5'''). HR-MS: calcd for C₂₆H₂₆N₂O₂ [$M + H$]⁺: 399.2073; found: 399.2059. MS: (EI, 200 °C) m/z 398.4 (M^+ 54%); Anal. calcd for C₂₆H₂₆N₂O₂: C 78.36, H 6.58, N 7.03; found: C 78.06, H 6.87, N 7.16.

4.2.2.3. 4'-((2-Pentyl-1H-benzo[d]imidazol-1-yl)methyl)-[1,1'-biphenyl]-2-carbamide (**2-B**).

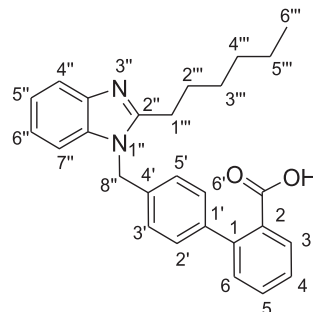


Beige-colored powder; yield 0.04 g (0.10 mmol, 11%); mp 152 °C.

$^1\text{H-NMR}$ (400 MHz/DMSO- d_6): δ 7.63 (s, 1H, NH), 7.59 (m, 1H,

H4''), 7.50 (m, 1H, H7''), 7.44 (ddd, 1H, H4), 7.41 (d, 1H, H3), 7.39 (ddd, 1H, H5), 7.37 (d, $^3J = 8.3$ Hz, 2H, H2' + H6'), 7.31 (dd, 1H, H6), 7.25 (s, 1H, NH), 7.16 (m, 2H, H5'' + H6''), 7.11 (d, $^3J = 8.3$ Hz, 2H, H3' + H5'), 5.52 (s, 2H, CH₂ 8''), 2.85 (t, 2H, CH₂ 1'''), 1.76 (tt, 2H, CH₂ 2'''), 1.31 (m, 4H, CH₂ 3'''' + CH₂ 4'''), 0.84 (t, 3H, CH₃ 5'''). MS: (EI, 100 °C) m/z 397.4 (M^+ 58%); Anal. calcd for C₂₆H₂₇N₃O: C 78.56, H 6.85, N 10.57; found: C 78.57, H 6.61, N 10.32.

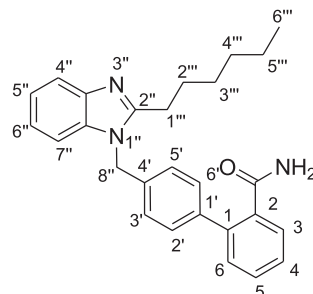
4.2.2.4. 4'-((2-Hexyl-1H-benzo[d]imidazol-1-yl)methyl)-[1,1'-biphenyl]-2-carboxylic acid (**2-C**).



Beige-colored powder; yield 0.08 g (0.19 mmol, 21%); mp 194 °C.

$^1\text{H-NMR}$ (400 MHz/DMSO- d_6): δ 12.75 (s, 1H, COOH), 7.70 (dd, 1H, H3), 7.59 (m, 1H, H4''), 7.53 (ddd, 1H, H5), 7.50 (m, 1H, H7''), 7.43 (ddd, 1H, H4), 7.31 (dd, 1H, H6), 7.28 (d, $^3J = 8.3$ Hz, 2H, H2' + H6'), 7.16 (m, 2H, H5'' + H6''), 7.12 (d, $^3J = 8.3$ Hz, 2H, H3' + H5'), 5.53 (s, 2H, CH₂ 8''), 2.85 (t, $^3J = 7.5$ Hz, 2H, CH₂ 1'''), 1.74 (tt, $^3J = 7.5$ Hz, 2H, CH₂ 2'''), 1.35 (m, 2H, CH₂ 3'''), 1.24 (m, 4H, CH₂ 4'''' + CH₂ 5'''), 0.83 (t, 3H, CH₃). $^{13}\text{C-NMR}$ (200 MHz, DMSO- d_6) δ 170.11, 155.76, 142.91, 140.91, 140.59, 136.61, 135.92, 132.91, 131.32, 130.93, 129.62, 129.21, 127.84, 126.79, 122.23, 121.86, 119.00, 110.69, 46.25, 31.55, 28.94, 27.44, 27.15, 22.53, 14.48. HR-MS: calcd for C₂₇H₂₈N₂O₂ [$M + H$]⁺: 413.2273; found: 413.2219. MS: (EI, 150 °C) m/z 412.2 (M^+ 55%); Anal. calcd for C₂₇H₂₈N₂O₂: C 78.61, H 6.84, N 6.79; found: C 78.70, H 7.02, N 6.91.

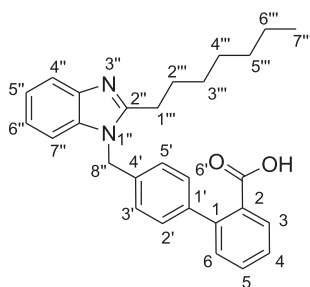
4.2.2.5. 4'-((2-Hexyl-1H-benzo[d]imidazol-1-yl)methyl)-[1,1'-biphenyl]-2-carbamide (**2-D**).



Beige-colored powder; yield 0.04 g (0.10 mmol, 11%); mp 154 °C.

$^1\text{H-NMR}$ (400 MHz/DMSO- d_6): δ 7.63 (s, 1H, NH), 7.59 (m, 1H, H4''), 7.50 (m, 1H, H7''), 7.44 (ddd, 1H, H4), 7.41 (d, 1H, H3), 7.39 (ddd, 1H, H5), 7.37 (s, 1H, NH), 7.16 (m, 2H, H5'' + H6''), 7.11 (d, $^3J = 8.3$ Hz, 2H, H3' + H5'), 5.52 (s, 2H, CH₂ 8''), 2.86 (t, $^3J = 7.4$ Hz, 2H, CH₂ 1'''), 1.76 (tt, $^3J = 7.4$ Hz, 2H, CH₂ 2'''), 1.35 (m, 2H, CH₂ 3'''), 1.25 (m, 4H, CH₂ 4'''' + CH₂ 5'''), 0.84 (t, 3H, CH₃ 6'''). MS: (EI, 200 °C) m/z 411.3 (M^+ 46%); Anal. calcd for C₂₇H₂₉N₃O: C 78.80, H 7.10, N 10.21; found: C 78.97, H 7.35, N 10.18.

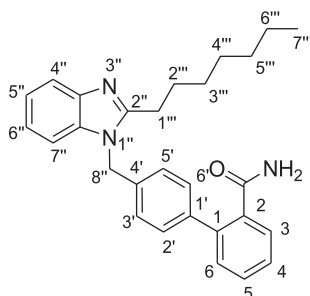
4.2.2.6. 4'-((2-Heptyl-1H-benzo[d]imidazol-1-yl)methyl)-[1,1'-biphenyl]-2-carboxylic acid (**2-E**).



Colorless crystals; yield 0.07 g (0.16 mmol, 19%); mp 172 °C.

$^1\text{H-NMR}$ (400 MHz/DMSO- d_6): δ 12.75 (s, 1H, COOH), 7.66 (d, 1H, H3), 7.59 (m, 1H, H4''), 7.50 (m, 2H, H5+H7''), 7.41 (ddd, 1H, H4), 7.30 (d, 1H, H6), 7.29 (d, $^3J = 8.1$ Hz, 2H, H2' + H6'), 7.16 (m, 1H, H5'' + H6''), 7.11 (d, $^3J = 8.1$ Hz, 2H, H3' + H5'), 5.52 (s, 2H, CH₂ 8''), 2.85 (t, $^3J = 7.5$ Hz, 2H, CH₂ 1'''), 1.73 (tt, $^3J = 7.5$ Hz, 2H, CH₂ 2'''), 1.29 (m, 8H, CH₂ 3''' + CH₂ 4''' + CH₂ 5''' + CH₂ 6'''), 0.83 (t, 3H, CH₃ 7'''). $^{13}\text{C NMR}$ (200 MHz, DMSO- d_6) δ 170.38, 155.74, 142.90, 140.67, 136.49, 135.90, 130.96, 130.81, 129.49, 129.20, 127.75, 126.74, 122.22, 121.85, 118.99, 110.68, 46.25, 31.71, 29.23, 29.00, 27.48, 27.14, 22.61, 14.47. HR-MS: calcd for C₂₈H₃₀N₂O₂ [M+H]⁺: 427.2373; found: 427.2372. MS: (EI, 225 °C) m/z 426.3 (M⁺ 47%); Anal. calcd for C₂₈H₃₀N₂O₂ (x 0.5H₂O): C 77.21, H 7.17, N 6.43; found: C 77.57, H 7.34, N 6.53.

4.2.2.7. 4'-((2-Heptyl-1H-benzo[d]imidazol-1-yl)methyl)-[1,1'-biphenyl]-2-carbamide (**2-F**).



Colorless crystals; yield 0.05 g (0.12 mmol, 14%); mp 153 °C.

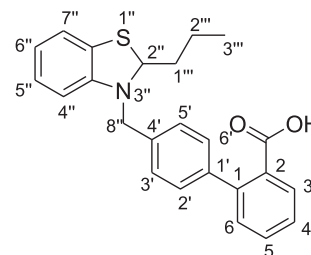
$^1\text{H-NMR}$ (400 MHz/DMSO- d_6): δ 7.62 (s, 1H, NH), 7.59 (m, 1H, H4''), 7.50 (m, 1H, H7''), 7.44 (ddd, 1H, H4), 7.41 (d, 1H, H3), 7.40 (ddd, 1H, H5), 7.37 (d, $^3J = 8.3$ Hz, 2H, H2' + H6'), 7.31 (d, 1H, H6), 7.23 (s, 1H, NH), 7.16 (m, 2H, H5'' + H6''), 7.11 (d, $^3J = 8.3$ Hz, 2H, H3' + H5'), 5.51 (s, 2H, CH₂ 8''), 2.85 (t, $^3J = 7.5$ Hz, 2H, CH₂ 1'''), 1.75 (tt, $^3J = 7.5$ Hz, 2H, CH₂ 2'''), 1.29 (m, 8H, CH₂ 3''' + CH₂ 4''' + CH₂ 5''' + CH₂ 6'''), 0.84 (t, 3H, CH₃ 7'''). HR-MS: calcd for C₂₈H₃₁N₃O [M+H]⁺: 426.2573; found: 426.2533. MS: (EI, 150 °C) m/z 425.4 (M⁺ 40%).

4.2.3. Hydrolysis reaction of 4'-((2-propyl-2,3-dihydro-1,3-benzo[d]thiazol-3-yl)methyl)-[1,1'-biphenyl]-2-carbonitrile

4'-((2-Propyl-2,3-dihydro-1,3-benzo[d]thiazol-3-yl)methyl)-[1,1'-biphenyl]-2-carbonitrile **8** (0.35 g, 0.94 mmol) was dissolved in 15 ml of methanol and combined with 5.30 ml of KOH (30%) (28.3 mmol). The mixture was heated to reflux for 14d. After cooling to RT, HCl was added until the solution was acidified. Subsequently, the crude product was isolated by extraction with methylene chloride. After drying over Na₂SO₄, the solvent was removed in vacuo and the products (**3-A** and **3-B**) were separated

by column chromatography on silica gel with diethyl ether/methanol (95:5) and recrystallized from diethyl ether/methanol.

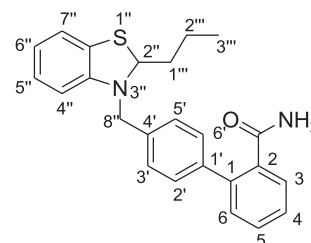
4.2.3.1. 4'-((2-Propyl-2,3-dihydro-1,3-benzo[d]thiazol-3-yl)methyl)-[1,1'-biphenyl]-2-carboxylic acid (**3-A**).



Brown solid; yield (diastereomer 1 + 2): 0.06 g (0.15 mmol, 16%); mp 83 °C.

$^1\text{H-NMR}$ (400 MHz/DMSO- d_6): δ (diastereomer 1) 12.79 (s, 1H, COOH), 7.68 (d, 1H, H3), 7.56 (ddd, 1H, H4), 7.44 (ddd, 1H, H5), 7.38 (d, 1H, H6), 7.35 (d, $^3J = 8.2$ Hz, 2H, H2' + H6'), 7.28 (d, $^3J = 8.2$ Hz, 2H, H3' + H5'), 6.90 (dd, 1H, H7''), 6.86 (ddd, 1H, H5''), 6.70 (dd, 1H, H4''), 6.49 (ddd, 1H, H6''), 6.14 (s, broad, 1H, CH₂ 8''), 4.11 (d, 1H, CH₂ 8''), 3.53 (m, 1H, H2''), 1.54–1.30 (m, 4H, CH₂ 1''' + CH₂ 2'''), 0.83 (t, 3H, CH₃ 3'''). $^1\text{H-NMR}$ (400 MHz/DMSO- d_6): δ (diastereomer 2) 12.79 (s, 1H, COOH), 7.68 (d, 1H, H3), 7.54 (ddd, 1H, H4), 7.43 (ddd, 1H, H5), 7.38 (d, 1H, H6), 7.28 (d, 2H, H2' + H6'), 7.23 (d, $^3J = 8.3$ Hz, 2H, H3' + H5'), 6.90 (dd, 1H, H7''), 6.86 (ddd, 1H, H5''), 6.73 (dd, 1H, H4''), 6.54 (ddd, 1H, H6''), 6.01 (s, broad, 1H, CH₂ 8''), 4.45 (d, 1H, CH₂ 8''), 3.69 (m, 1H, H2''), 1.54–1.30 (m, 4H, CH₂ 1''' + CH₂ 2'''), 0.83 (t, 3H, CH₃ 3'''). HR-MS: calcd for C₂₄H₂₃NO₂S [M+H]⁺: 390.1473; found: 390.1511. MS: (EI, 175 °C) m/z 389.3 (M⁺ 95%).

4.2.3.2. 4'-((2-Propyl-2,3-dihydro-1,3-benzo[d]thiazol-3-yl)methyl)-[1,1'-biphenyl]-2-carbamide (**3-B**).



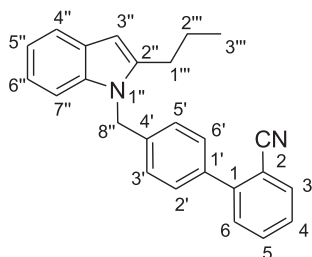
Colorless crystals; yield 0.03 g (0.08 mmol, 9%); mp 106 °C.

$^1\text{H-NMR}$ (400 MHz/DMSO- d_6): δ (diastereomer 1) 7.64 (s, 1H, NH), 7.49–7.37 (m, 4H, H3+H4+H5+H6), 7.36 (m, 4H, H2' + H3' + H5' + H6'), 7.29 (s, 1H, NH), 6.92 (dd, 1H, H7''), 6.86 (ddd, 1H, H5''), 6.70 (dd, 1H, H4''), 6.49 (ddd, 1H, H6''), 6.10 (d, 1H, CH₂ 8''), 4.10 (d, 1H, CH₂ 8''), 3.53 (m, 1H, H2''), 1.55–1.29 (m, 4H, CH₂ 1''' + CH₂ 2'''), 0.84 (t, 3H, CH₃ 3'''). $^1\text{H-NMR}$ (400 MHz/DMSO- d_6): δ (diastereomer 2) 7.64 (s, 1H, NH), 7.49–7.37 (m, 4H, H3+H4+H5+H6), 7.36 (m, 4H, H2' + H3' + H5' + H6'), 7.29 (s, 1H, NH), 6.92 (dd, 1H, H7''), 6.86 (ddd, 1H, H5''), 6.73 (dd, 1H, H4''), 6.54 (ddd, 1H, H6''), 6.00 (s, broad, 1H, CH₂ 8''), 4.43 (d, 1H, CH₂ 8''), 3.68 (m, 1H, H2''), 1.55–1.29 (m, 4H, CH₂ 1''' + CH₂ 2'''), 0.84 (t, 3H, CH₃ 3'''). MS: (EI, 150 °C) m/z 388.4 (M⁺ 66%).

4.2.4. 4'-((2-Propyl-1H-indol-1-yl)methyl)-[1,1'-biphenyl]-2-carbonitrile (**3-E**)

2-Propyl-1H-indole **11** (0.20 g, 5.02 mmol) in 10 ml of abs. DMF was carefully reacted with NaH (60% dispersion in mineral oil) (0.18 g, 4.46 mmol) while cooling in an ice bath. After the gas

formation stopped, 4'-bromomethyl-[1,1'-biphenyl]-2-carbonitrile (0.76 g, 2.76 mmol) dissolved in 2 ml of abs. DMF was added dropwise and the solution was stirred for 1 h under cooling in an ice bath and further 2 h at RT. Water was added and after the solution was acidified with HCl, the product was extracted three times with methylene chloride. The combined organic layers were dried over Na₂SO₄ and evaporated to dryness in vacuo. The crude product was purified by column chromatography on silica gel with ethyl acetate/n-hexane (1:3).



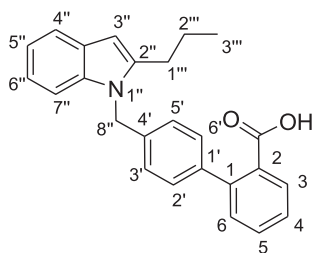
Yellow oil; yield 0.50 g (1.43 mmol, 57%).

¹H-NMR (400 MHz/DMSO-*d*₆): δ 7.92 (dd, 1H, H₃), 7.75 (ddd, 1H, H₅), 7.57 (d, 1H, H₆), 7.55 (ddd, 1H, H₄), 7.50 (m, 1H, H_{7''}), 7.50 (d, 2H, H_{2'} + H_{6'}), 7.38 (dd, ⁴J = 0.7 Hz, 1H, H_{4''}), 7.09 (d, 2H, H_{3'} + H_{5'}), 7.04 (ddd, 1H, H_{5''}), 6.99 (ddd, 1H, H_{6''}), 6.11 (d, ⁴J = 0.7 Hz, 1H, H_{3''}), 5.51 (s, 2H, CH₂ 8''), 2.7 (t, ³J = 7.5 Hz, 2H, CH₂ 1'''), 1.68 (tq, ³J = 7.5 Hz, ³J = 7.4 Hz, 2H, CH₂ 2'''), 0.97 (t, ³J = 7.4 Hz, 3H, CH₃ 3'''). MS: (EI, 75 °C) *m/z* 350.5 (M⁺ 88%); Anal. calcd for C₂₅H₂₂N₂: C 85.68, H 6.33, N 7.99; found: C 85.70, H 6.39, N 8.07.

4.2.5. Hydrolysis reaction of 4'-((2-propyl-1H-indol-1-yl)methyl)-[1,1'-biphenyl]-2-carbonitrile

4'-((2-Propyl-1H-indol-1-yl)methyl)-[1,1'-biphenyl]-2-carbonitrile (0.35 g, 1.00 mmol) **3-E** was dissolved in 15 ml of methanol and combined with 5.61 ml of KOH (30%) (30 mmol). The mixture was heated to reflux for 24d. After cooling to RT, HCl was added until the solution was acidified. Subsequently, the crude product was isolated by extraction with methylene chloride. After drying over Na₂SO₄, the solvent was removed in vacuo and the products (**3-C** and **3-D**) were separated by column chromatography on silica gel with methylene chloride/methanol (95:5) and recrystallized from diethyl ether/methanol.

4.2.5.1. 4'-((2-Propyl-1H-indol-1-yl)methyl)-[1,1'-biphenyl]-2-carboxylic acid (**3-C**).

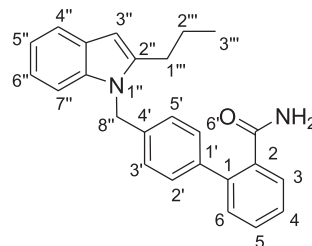


Brown oil, yield 0.06 g (0.16 mmol, 16%).

¹H-NMR (400 MHz/DMSO-*d*₆): δ 12.75 (s, 1H, COOH), 7.67 (dd, 1H, H₃), 7.52 (dd, 1H, H₅), 7.49 (d, 1H, H_{7''}), 7.42 (ddd, 1H, H₄), 7.37 (d, 1H, H_{4''}), 7.32 (dd, 1H, H₆), 7.24 (d, ³J = 8.1 Hz, 2H, H_{2'} + H_{6'}), 7.03 (ddd, 1H, H_{5''}), 7.00 (m, 1H, H_{6''}), 6.98 (d, ³J = 8.1 Hz, 2H, H_{3'} + H_{5'}), 6.32 (d, 1H, H_{3''}), 5.46 (s, 2H, CH₂ 8''), 2.69 (t, ³J = 7.5 Hz, 2H, CH₂ 1'''), 1.69 (tq, ³J = 7.5 Hz, ³J = 7.4 Hz, 2H, CH₂ 2'''), 0.97 (t, ³J = 7.4 Hz, 3H, CH₃ 3'''). HR-MS: calcd for C₂₅H₂₃NO₂ [M+H]⁺:

370.1773; found: 370.1797. MS: (EI, 150 °C) *m/z* 369.4 (M⁺ 92%); Anal. calcd for C₂₅H₂₃NO₂ (x 0.5H₂O): C 79.34, H 6.39, N 3.70; found: C 79.04, H 6.36, N 3.92.

4.2.5.2. 4'-((2-Propyl-1H-indol-1-yl)methyl)-[1,1'-biphenyl]-2-carbamid (**3-D**).



White solid, yield 0.04 g (0.11 mmol, 11%); mp 196 °C.

¹H-NMR (400 MHz/DMSO-*d*₆): δ 7.62 (s, 1H, NH), 7.49 (dd, 1H, H_{7''}), 7.44 (ddd, 1H, H₄), 7.38 (d, 1H, H_{4''}), 7.38 (ddd, 1H, H₅), 7.35 (d, 1H, H₃), 7.31 (d, 1H, H₆), 7.33 (d, ³J = 8.2 Hz, 2H, H_{2'} + H_{6'}), 7.25 (s, 1H, NH), 7.03 (ddd, 1H, H_{5''}), 7.00 (ddd, 1H, H_{6''}), 6.96 (d, ³J = 8.2 Hz, 2H, H_{3'} + H_{5'}), 6.32 (s, 1H, H_{3''}), 5.45 (s, 2H, CH₂ 8''), 2.70 (t, ³J = 7.6 Hz, 2H, CH₂ 1'''), 1.70 (tq, ³J = 7.6 Hz, ³J = 7.4 Hz, 2H, CH₂ 2'''), 0.98 (t, ³J = 7.4 Hz, 3H, CH₃ 3'''). MS: (EI, 150 °C) *m/z* 368.4 (M⁺ 73%); Anal. calcd for C₂₅H₂₄N₂O: C 81.49, H 6.57, N 7.60; found: C 81.69, H 6.53, N 7.54.

4.3. Biology

4.3.1. General cell culture methods

The mouse embryonic 3T3-L1 cell line, the monkey kidney-derived COS-7 cell line and the human prostate adenoma cell line LNCaP were obtained from the American Type Culture Collection (ATCC). The 3T3-L1 and the COS-7 cells were maintained as monolayer cultures in Dulbecco's modified Eagle medium (DMEM) with phenol red, 4.5 g/l glucose, 584 mg/l L-glutamine (GE Healthcare), supplemented with fetal calf serum (FCS, 10%; Biobrom). LNCaP cells were cultivated as monolayer culture in poly-D-lysine treated culture vessels in RPMI 1640 without phenol red (GE Healthcare), supplemented with FCS (10%) and L-glutamine (584 mg/l; GE Healthcare). The cells were cultivated in a humidified atmosphere (5% CO₂/95% air) at 37 °C and passaged once (LNCaP) or twice (COS-7, 3T3-L1) a week.

4.3.2. PPAR_γ transactivation assay

Transient transfection (Lipofectamin 2000; Life Technologies) and dual-luciferase reporter assay (Promega) were performed according to the manufacturer's protocol. COS-7 cells were seeded in 96-well microtiter plates at a density of 10⁴ cells/well in completed DMEM and incubated at 37 °C and 5% CO₂ for 24 h prior to transfection. After changing to serum- and antibiotic-free medium, cells were transiently transfected with pGal5-TK-Luc (30 ng), pGal4-PPAR_γ-LBD (3 ng) and pRenilla-CMV (1 ng) in OptiMEM (25 μl; Gibco). After 4 h, the selected compounds, pioglitazone or vehicle (DMSO) were added at indicated concentrations, and luciferase activity was measured after 42 h.

4.3.3. 3T3-L1 differentiation assay

3T3-L1 preadipocytes were differentiated by a modified protocol previously described [19]. 3T3-L1 cells were seeded in 6-well plates and in a postconfluent state treated with completed DMEM containing insulin (0.17 μM) and dexamethasone (1 μM). After 3 days, medium was changed to completed DMEM containing insulin (0.17 μM) and incubated for further 3 days. Subsequently, cells were

incubated with solely completed medium for 3 more days. During the whole incubation period, the medium contained pioglitazone, telmisartan, vehicle DMSO, or the compounds at two different concentrations (1 μM and 10 μM), respectively. At day 9 of differentiation, cells were washed with phosphate buffered saline (PBS) and intracellular triglycerides were stained with Oil-Red O for 1 h. Intracellularly bound dye was extracted with isopropanol 80% and the absorbance of the extraction solution was measured at 515 nm.

4.3.4. *In vitro* chemosensitivity assay

The *in vitro* testing of the new compounds for their growth inhibitory activity on prostate adenocarcinoma cells and healthy COS-7 cells was carried out according to a modified protocol previously described [40,41]. LNCaP prostate adenocarcinoma cells (5×10^4 cells/well) and COS-7 cells (3×10^4 cells/well) were seeded in their exponential growth phase in complete DMEM in 96-well microtiter plates, which were in case of LNCaP cells previously coated with poly-D-lysine. Plates were kept at 37 °C for 24 h prior to addition of complete medium containing the appropriate concentration (final concentration 50 μM) of pioglitazone, telmisartan, vehicle DMSO, or compounds, respectively. After an incubation time of 72 h, medium was aspirated, cells were washed with PBS and fixed with a solution of 1% (v/v) glutaric acid in PBS. Cell biomass was determined via staining of the chromatin of adherent cells with crystal violet and subsequent measurement of absorbance at 590 nm. Cell viability is expressed as percentage of cell viability of vehicle-treated control which was set at 100%. Results are the mean \pm SD of at least two independent experiments. The IC₅₀ values were calculated with Prism 7 (GraphPad, San Diego, CA) using nonlinear regression and the log of the inhibitor versus variable slope response equation. The bottom constraint was set to 0%.

4.4. Docking

Docking studies with the synthesized PPAR γ modulators were performed using GOLD Suite v5.2.2 [42]. Default settings were applied and the GoldScore [43] selected as scoring function. Before docking the protein crystal structure of PPAR γ co-crystallized with telmisartan (PDB code: 3VN2 [44]) was prepared using MOE 2014.09 [45]. All waters with exception of those located in the binding site (HOH645, HOH625, HOH613 and HOH632) were removed. Next, hydrogens were added using the protonate 3D application with standard parameters. All compounds were docked into the PPAR γ binding site and ten poses per molecule retrieved. All ligand poses were minimized in the binding site using the MMFF94 force field. The resulting poses were then further inspected using LigandScout 3.12 and selected using a telmisartan-derived 3D pharmacophore as customized scoring function [46–48].

Acknowledgements

We thank Alexandra Knox (Department of Pharmaceutical Chemistry, University of Innsbruck) for recording the ¹³C-NMR spectra and Monika Cziferszky (Department of Pharmaceutical Chemistry, University of Innsbruck) for carrying out the high resolution mass analyses. This work was supported by Research Grant Gu 285/7-2 and Ki 712/3-2 from the Deutsche Forschungsgemeinschaft.

Appendix A. Supplementary data

Supplementary data associated with this article can be found in the online version, at <http://dx.doi.org/10.1016/j.ejmech.2016.08.027>. These data include MOL files and InChIKeys of the most

important compounds described in this article.

References

- [1] M. Lehrke, M.A. Lazar, The many faces of PPAR γ , *Cell* 123 (2005) 993–999.
- [2] N.J. McKenna, B.W. O'Malley, Combinatorial control of gene expression by nuclear receptors and coregulators, *Cell* 108 (2002) 465–474.
- [3] N. Viswakarma, Y. Jia, L. Bai, A. Vluggens, J. Borensztajn, J. Xu, J.K. Reddy, Coactivators in PPAR-regulated gene expression, *PPAR Res.* 2010 (2010). Article ID 250126.
- [4] P. Tontonoz, B.M. Spiegelman, Fat and beyond: The diverse biology of PPAR γ , *Annu. Rev. Biochem.* 77 (2008) 289–312.
- [5] T.A. Cock, S.M. Houten, J. Auwerx, Peroxisome proliferator-activated receptor γ : too much of a good thing causes harm, *EMBO Rep.* 5 (2004) 142–147.
- [6] E.J. Murphy, T.J. Davern, A.O. Shakil, L. Shick, U. Masharani, H. Chow, C. Freise, W.M. Lee, N.M. Bass, Troglitazone-induced fulminant hepatic failure. Acute liver failure study group, *Dig. Dis. Sci.* 3 (2000) 549–553.
- [7] A.M. Gallagher, L. Smeeth, S. Seabroke, H.G.M. Leufkens, T.P. van Staa, Risk of death and cardiovascular outcomes with thiazolidinediones: a study with the general practice research database and secondary care data, *PLoS One* 6 (2011) e28157.
- [8] J.D. Lewis, A. Ferrara, T. Peng, M. Hedderson, W.B. Bilker, C.P. Quesenberry, D.J. Vaughn, L. Nessel, J. Selby, B.L. Strom, Risk of bladder cancer among diabetic patients treated with pioglitazone: interim report of a longitudinal cohort study, *Diabetes Care* 34 (2011) 916–922.
- [9] M. Ahmadian, J.M. Suh, N. Hah, C. Liddle, A.R. Atkins, M. Downes, R.M. Evans, PPAR γ signaling and metabolism: the good, the bad and the future, *Nat. Med.* 9 (2013) 557–566.
- [10] H.P. Koeffler, Peroxisome proliferator-activated receptor γ and cancers, *Clin. Cancer Res.* 9 (2003) 1–9.
- [11] D. Shao, S.M. Rangwala, S.T. Bailey, S.L. Krakow, M.J. Reginato, M.A. Lazar, Interdomain communication regulating ligand binding by PPAR γ , *Nature* 396 (1998) 377–380.
- [12] G. Venkatachalam, A.P. Kumar, K.R. Sakharkar, S. Thangavel, M.-V. Clement, M.K. Sakharkar, PPAR γ disease gene network and identification of therapeutic targets for prostate cancer, *J. Drug Target.* 19 (2011) 781–796.
- [13] S. Sikka, L. Chen, G. Sethi, A.P. Kumar, Targeting PPAR γ signaling cascade for the prevention and treatment of prostate cancer, *PPAR Res.* 2012 (2012). Article ID 968040.
- [14] P.S. Nelson, N. Clegg, H. Arnold, C. Ferguson, M. Bonham, J. White, L. Hood, B. Lin, The program of androgen-responsive genes in neoplastic prostate epithelium, *Proc. Natl. Acad. Sci.* 99 (2002) 11890–11895.
- [15] T. Kubota, K. Koshizuka, E.A. Williamson, H. Asou, J.W. Said, S. Holden, I. Miyoshi, H. Phillip Koeffler, Ligand for peroxisome proliferator-activated receptor γ (troglitazone) has potent antitumor effect against human prostate cancer both in vitro and in vivo, *Cancer Res.* 58 (1998) 3344–3352.
- [16] D.J. Kojetin, T.P. Burris, Small molecule modulation of nuclear receptor conformational dynamics: implications for function and drug discovery, *Mol. Pharmacol.* 83 (2013) 1–8.
- [17] J.B. Bruning, M.J. Chalmers, S. Prasad, S.A. Busby, T.M. Kamenecka, Y. He, K.W. Nettles, P.R. Griffin, Partial agonists activate PPAR γ using a helix 12 independent mechanism, *Structure* 15 (2007) 1258–1271.
- [18] J.H. Choi, A.S. Banks, J.L. Estall, S. Kajimura, P. Bostrom, D. Laznik, J.L. Ruas, M.J. Chalmers, T.M. Kamenecka, M. Blüher, P.R. Griffin, B.M. Spiegelman, Anti-diabetic drugs inhibit obesity-linked phosphorylation of PPAR γ by Cdk5, *Nature* 466 (2010) 451–456.
- [19] M. Schupp, J. Janke, R. Clasen, T. Unger, U. Kintscher, Angiotensin type 1 receptor blockers induce peroxisome proliferator-activated receptor γ activity, *Circulation* 109 (2004) 2054–2057.
- [20] M. Schupp, M. Clemenz, R. Gineste, H. Witt, J. Janke, S. Helleboid, N. Hennuyer, P. Ruiz, T. Unger, B. Staels, U. Kintscher, Molecular characterization of new selective peroxisome proliferator-activated receptor γ modulators with angiotensin receptor blocking activity, *Diabetes* 54 (2005) 3442–3452.
- [21] S.C. Benson, H.A. Pershadsingh, C.I. Ho, A. Chittiboyina, P. Desai, M. Pravenec, N. Qi, J. Wang, M.A. Avery, T.W. Kurtz, Identification of telmisartan as a unique angiotensin II receptor antagonist with selective PPAR γ -modulating activity, *Hypertension* 43 (2004) 993–1002.
- [22] M. Matsuyama, R. Yoshimura, Peroxisome proliferator-activated receptor γ is a potent target for prevention and treatment in human prostate and testicular cancer, *PPAR Res.* 2008 (2008).
- [23] H. Ishiguro, Y. Ishiguro, Y. Kubota, H. Uemura, Regulation of prostate cancer cell growth and PSA expression by angiotensin II receptor blocker with peroxisome proliferator-activated receptor γ ligand like action, *Prostate* 67 (2007) 924–932.
- [24] M. Goebel, M. Clemenz, B. Staels, T. Unger, U. Kintscher, R. Gust, Characterization of new PPAR γ agonists: analysis of telmisartan's structural components, *ChemMedChem* 4 (2009) 445–456.
- [25] M. Goebel, G. Wolber, P. Markt, B. Staels, T. Unger, U. Kintscher, R. Gust, Characterization of new PPAR γ agonists: benzimidazole derivatives — importance of positions 5 and 6, and computational studies on the binding mode, *Bioorg. Med. Chem.* 18 (2010) 5885–5895.
- [26] L. Herbst, M. Goebel, S. Bandholtz, R. Gust, U. Kintscher, Characterization of telmisartan-derived PPAR γ agonists: importance of moiety shift from position 6 to 5 on potency, efficacy and cofactor recruitment, *ChemMedChem* 7 (2012)

- 1935–1942.
- [27] M. Goebel, B. Staels, T. Unger, U. Kintscher, R. Gust, Characterization of new PPAR γ agonists: benzimidazole derivatives – the importance of position 2, *ChemMedChem* 4 (2009) 1136–1142.
- [28] D.N. Korolev, N.A. Bumagin, An improved protocol for ligandless Suzuki–Miyaura coupling in water, *Tetrahedron Lett.* 47 (2006) 4225–4229.
- [29] C. Djerassi, Brominations with N-bromosuccinimide and related compounds. The Wohl-Ziegler reaction, *Chem. Rev.* 43 (1948) 271–317.
- [30] K.C. Santhosh, G.C. Paul, E. De Clercq, C. Pannecouque, M. Witvrouw, T.L. Loftus, J.A. Turpin, R.W. Buckheit, M. Cushman, Correlation of anti-HIV activity with anion spacing in a series of cosalane analogues with extended polycarboxylate pharmacophores, *J. Med. Chem.* 44 (2001) 703–714.
- [31] M.A. Phillips, The formation of 2-substituted benzimidazoles, *J. Chem. Soc.* 13 (1928) 2393–2399.
- [32] D.V. Ramana, E. Kantharaj, Mass spectrometer as a probe in the synthesis of 2-substituted benzimidazoles, *Tetrahedron Lett.* 50 (1994) 2485–2496.
- [33] L. Capuano, A. Ahlhelm, H. Hartmann, New syntheses of 2-acylbenzofurans, 2-acylindoles, 2-indolylcarboxylates and 2-quinolones by intramolecular Wittig reaction, *Chem. Ber.* 119 (1986) 2069–2074.
- [34] S. Taira, H. Danjo, T. Imamoto, A facile synthesis of 2-substituted indoles from (2-aminobenzyl)triphenylphosphonium salts, *Tetrahedron Lett.* 43 (2002) 2885–2888.
- [35] J.O. Nwankwo, M.E.C. Robbins, Peroxisome proliferator-activated receptor γ expression in human malignant and normal brain, breast and prostate-derived cells, *Prostagl. Leukot. Essent. Fat. Acids* 64 (2001) 241–245.
- [36] Y. Amano, T. Yamaguchi, K. Ohno, T. Niimi, M. Orita, H. Sakashita, M. Takeuchi, Structural basis for telmisartan-mediated partial activation of PPAR γ , *Hypertens. Res.* 35 (2012) 715–719.
- [37] P. Markt, R.K. Petersen, E.N. Flindt, K. Kristiansen, J. Kirchmair, G. Spitzer, S. Distinto, D. Schuster, G. Wolber, C. Laggner, T. Langer, Discovery of novel PPAR ligands by a virtual screening approach based on pharmacophore modeling, 3D shape, and electrostatic similarity screening, *J. Med. Chem.* 51 (2008) 6303–6317.
- [38] L. Guasch, E. Sala, A. Castell-Auví, L. Cedó, K.R. Liedl, G. Wolber, M. Muehlbacher, M. Mulero, M. Pinent, A. Ardévol, C. Valls, G. Pujadas, S. Garcia-Vallvé, Identification of PPAR γ partial agonists of natural origin (I): development of a virtual screening procedure and in vitro validation, *PLoS One* 7 (2012) e50816.
- [39] R.B. El-Houri, J. Mortier, M.S. Murgueitio, G. Wolber, L.P. Christensen, Identification of PPAR γ agonists from natural sources using different in silico approaches, *Planta Med.* 81 (2015) 488–494.
- [40] H. Reile, H. Birnböck, G. Bernhardt, T. Spruss, H. Schönenberger, Computerized determination of growth kinetic curves and doubling times from cells in microculture, *Anal. Biochem.* 187 (1990) 262–267.
- [41] G. Bernhardt, H. Reile, H. Birnböck, T. Spruss, H. Schönenberger, Standardized kinetic microassay to quantify differential chemosensitivity on the basis of proliferative activity, *J. Cancer Res. Clin. Oncol.* 118 (1992) 35–43.
- [42] GOLD Suite v5.2.2, in, *Cambridge Crystallographic Data Centre*, Cambridge, UK, 2013.
- [43] M.L. Verdonk, J.C. Cole, M.J. Hartshorn, C.W. Murray, R.D. Taylor, Improved protein–ligand docking using GOLD, *Proteins* 52 (2003) 609–623.
- [44] Y. Amano, T. Yamaguchi, K. Ohno, T. Niimi, M. Orita, H. Sakashita, M. Takeuchi, Structural basis for telmisartan-mediated partial activation of PPAR γ , *Hypertens. Res.* 35 (2012) 715–719.
- [45] Molecular Operating Environment (MOE), 2014.09, in, *Chemical Computing Group Inc.*, 1010 Sherbooke St. West, Suite #910, Montreal, QC, Canada, H3A 2R7, 2015.
- [46] T. Seidel, G. Ibis, F. Bendix, G. Wolber, Strategies for 3D pharmacophore-based virtual screening, *Drug Discov. Today Technol.* 7 (2010) e221–e228.
- [47] G. Wolber, A.A. Dornhofer, T. Langer, Efficient overlay of small organic molecules using 3D pharmacophores, *J. Comp. Aided Mol. Des.* 20 (2006) 773–788.
- [48] G. Wolber, T. Langer, LigandScout: 3-d pharmacophores derived from protein-bound ligands and their use as virtual screening filters, *J. Chem. Inf. Model.* 45 (2005) 160–169.